Article

Influence of Hydroxylation, Chain Length, and Chain Unsaturation on Bilayer Properties of Ceramides

Terhi Maula,[1,*] Md. Abdullah Al Sazzad,[1] and J. Peter Slotte[1]
[1]Biochemistry, Faculty of Science and Engineering, Åbo Akademi University, Turku, Finland

ABSTRACT Mammalian ceramides constitute a family of at least a few hundred closely related molecules distinguished by small structural differences, giving rise to individual molecular species that are expressed in distinct cellular compartments, or tissue types, in which they are believed to execute distinct functions. We have examined how specific structural details influence the bilayer properties of a selection of biologically relevant ceramides in mixed bilayers together with sphingomyelin, phosphatidylcholine, and cholesterol. The ceramide structure varied with regard to interfacial hydroxylation, the identity of the headgroup, the length of the *N*-acyl chain, and the position of *cis*-double bonds in the acyl chains. The interactions of the ceramides with sphingomyelin, their lateral segregation into ceramide-rich domains in phosphatidylcholine bilayers, and the effect of cholesterol on such domains were studied with DSC and various fluorescence-based approaches. The largest differences arose from the presence and relative position of *cis*-double bonds, causing destabilization of the ceramide's interactions and lateral packing relative to common saturated and hydroxylated species. Less variation was observed as a consequence of interfacial hydroxylation and the *N*-acyl chain length, although an additional hydroxyl in the sphingoid long-chain base slightly destabilized the ceramide's interactions and packing relative to a nonhydroxyceramide, whereas an additional hydroxyl in the *N*-acyl chain had the opposite effect. In conclusion, small structural details conferred variance in the bilayer behavior of ceramides, some causing more dramatic changes in the bilayer properties, whereas others imposed only fine adjustments in the interactions of ceramides with other membrane lipids, reflecting possible functional implications in distinct cell or tissue types.

INTRODUCTION

Ceramides, one of the simplest classes of sphingolipids, virtually comprise a large number of heterogeneous, yet structurally very closely related molecules produced in mammals by the six distinct ceramide synthases for which the tissue expression profiles seem to correlate with the acyl chain composition of the ceramides in the specific tissues (1,2). Besides their central role as immediate precursors of more complex sphingolipids, several lines of evidence point to a role for ceramides in cellular activities and signaling cascades (3-6). The local levels of ceramides in cells may be significantly increased (e.g., by activation of sphingomyelinases (7,8)). Being very hydrophobic, ceramides exhibit extremely low solubility in aqueous media such as the cellular cytosol, and are therefore expected to exert their effects on the level of membranes. Many biologically relevant ceramide species display high phase transition temperatures relative to other membrane lipid classes, making them solid-like molecules that have major influences on the physical properties of bilayer membranes. These range from altered thermodynamical behavior (9,10), to significant impacts on the molecular order and lateral distribution (11-19), as well as the topographical organization of membranes (20-25), often caused by the self-segregation of ceramides into highly ordered lateral domains in bilayers, and their tendency to induce negative membrane curvature. Ceramides thus affect the physical state of lipid bilayers, and along with the proposition that the membrane physical state could influence the physiological state of a cell (26,27), membrane phenomena induced by ceramides have also become a subject of intense study. Ceramides have been studied from both biological and biochemical, as well as from biophysical points of view, to understand the molecular properties of ceramides that affect their functions in distinct subcellular compartments, possibly influencing cell physiology.

In general, ceramides comprise a long-chain aminediol (sphingoid) base to which a fatty acyl moiety is amide(*N*)-linked. Natural ceramides display wide variation in the length of their *N*-linked acyl chains, with ever-increasing levels of diversification induced by unsaturation, hydroxylation and branching that may occur at different positions of the *N*-linked chain (28). In addition, variations in the chemical structure also occur in the sphingoid long-chain base of ceramides (29,30). With the aim of comparing the influence of selected structural aspects on the bilayer properties of ceramides, this study explores a set of biologically relevant ceramides in mixtures with other common membrane lipids. Although the ceramide's *N*-linked acyl chain may vary in length from 14 to 26 or even up to 36 carbon atoms as in skin ceramides (28,31,32), this study focuses on some of

Submitted June 2, 2015, and accepted for publication August 31, 2015.
*Correspondence: terhi.maula@abo.fi
Editor: Anne Kenworthy.

0006-3495/15/10/1639/13
http://dx.doi.org/10.1016/j.bpj.2015.08.040

the most prevalent mammalian molecular species, namely the saturated C16-, C18-, and C24-ceramides, as well as the monounsaturated C18:1$^{\Delta 9c}$- and C24:1$^{\Delta 15c}$-species (31,33-35), all containing the most prevalent mammalian sphingosine (18:1$^{\Delta 4t}$) long-chain base. In addition, two mammalian hydroxylated species of ceramides were studied: C18(2OH)-ceramide, (i.e., the [2′R]-isomer of the α-hydroxylated ceramide with a sphingosine long-chain base, and C16-phytoceramide with the [4′R]-hydroxysphinganine long-chain base (31,33,34,36,37)). Also the biologically potent metabolite ceramide-1-phosphate (38,39) (i.e., the product of ceramide kinase activity, and a ceramide containing a diunsaturated sphingadiene long-chain base [18:2$^{\Delta 4t,14c}$], which is found in human plasma and aorta (40,41)), were included in this study. To compare the effect of the somewhat uncommon *cis*-double bond in the sphingadiene long-chain base with a *cis*-double bond at a comparable bilayer depth in the *N*-acyl chain, a ceramide with an unsaturated C18:1$^{\Delta 12c}$ *N*-linked acyl chain was included in the study, although such a molecular species has not, according to the best of our knowledge, been reported among mammalian ceramide species. A complete description of the *N*-acyl chain and sphingoid base components of each of the ceramides are listed in Table 1, and the chemical structures of the ceramides are shown in Scheme S1 in the Supporting Material.

The phase behavior, miscibility, and bilayer properties of ceramides with varying structures have been previously studied as pure components or (mainly) in binary mixtures with sphingomyelin (SM) or phosphatidylcholines (PC) using DSC, NMR as well as fluorescence and monolayer techniques (9,14,42-50). This study, however, focuses on collecting comparable data for a variety of ceramide molecular species in various mixed bilayers together with palmitoyl sphingomyelin (PSM), 1-palmitoyl-2-oleoyl-*sn*-glycero-3-phosphocholine (POPC), and cholesterol. DSC together with various fluorescence-based approaches was applied to reveal differences in the miscibility of the ceramides with PSM and their lateral segregation in POPC bilayers. Fluorescence anisotropy and time-resolved intensity decays of *trans*-parinaric acid (tPA), a membrane probe that readily partitions into (highly) ordered phases such as ceramide-rich phases in lipid bilayers (15,17,51-53), were measured to determine the thermal stability and degree of lateral chain packing within ceramide-rich domains. Furthermore, as a multitude of evidence shows that ceramides and cholesterol exhibit reciprocal effects on each other's membrane lateral distribution (18,51,53-59), bilayer solubility (60,61), and affinity (62), also studied are the effect of cholesterol on the thermal stability of the ceramide-enriched domains and, using a fluorescence quenching approach that uses a fluorescent sterol-analog (63), cholesterol's exclusion from or incorporation into such domains.

Our results reveal that the largest differences within the ceramides, in terms of ceramide-PSM interactions and the formation of ceramide(/PSM)-enriched domains in POPC bilayers, arose from the presence and relative position of *cis*-double bonds in the ceramide acyl chains. Much less variation was observed in relation to the length of the (saturated) *N*-acyl chain or the presence of additional hydroxyls in the interfacial region. In conclusion, based on our results it appears that unsaturation cause more dramatic, although highly position-dependent, changes in the bilayer physical properties, whereas variations in the *N*-acyl chain length or presence of interfacial hydroxyls provide merely fine adjustments in the interactions of ceramides with other membrane lipids.

TABLE 1 Ceramide molecular species

Symbolic Notation	Systematic Name
C16-cer	*N*-palmitoyl-D-*erythro*-sphingosine
C18-cer	*N*-stearoyl-D-*erythro*-sphingosine
C24-cer	*N*-lignoceroyl-D-*erythro*-sphingosine
C16-phyto-cer	*N*-palmitoyl-D-*erythro*-4-hydroxysphinganine
C18(2OH)-cer	*N*-(2′(R)-hydroxy)-stearoyl-D-*erythro*-sphingosine
Cer-1-P	*N*-palmitoyl-D-*erythro*-sphingosine-1-phosphate
C18:1$^{\Delta 9c}$-cer	*N*-oleoyl-D-*erythro*-sphingosine
C24:1$^{\Delta 15c}$-cer	*N*-nervonoyl-D-*erythro*-sphingosine
C18:1$^{\Delta 12c}$-cer	*N*-12Z-octadecenoyl-D-*erythro*-sphingosine
C18-sphingadiene-cer	*N*-stearoyl-D-*erythro*-sphinga-4E,14Z-diene

For the chemical structures, see Scheme S1.

MATERIALS AND METHODS

POPC, *N*-stearoyl-D-*erythro*-sphingosine (C18-cer), *N*-oleoyl-D-*erythro*-sphingosine (C18:1$^{\Delta 9c}$-cer), *N*-(2′(R)-hydroxy)-stearoyl-D-*erythro*-sphingosine (C18:0(2OH)-cer), *N*-lignoceroyl-D-*erythro*-sphingosine (C24-cer), and *N*-nervonoyl-D-*erythro*-sphingosine (C24:1$^{\Delta 15c}$-cer) were purchased from Avanti Polar Lipids (Alabaster, AL); *N*-palmitoyl-D-*erythro*-sphingosine (C16-cer) and *N*-palmitoyl-D-*erythro*-phytosphingosine (C16-phytocer) from Larodan Fine Chemicals (Malmö, Sweden); and cholesterol from Sigma/Aldrich (St. Louis, MO). PSM was purified from egg yolk SM with preparative reverse-phase high-performance liquid chromatography (HPLC) as previously described (64), positively identified by mass spectrometry on a Bruker Daltonics Ion Trap ESI-MS (Bremen, Germany), and the purity verified by Merck/Hitachi LaChrome reverse-phase analytical HPLC (Supelco Discovery 125 × 4.6 mm C18-column with 5 μm particle size, Bellefonte, PA).

Ceramide-1-phosphate (Cer-1-P) was synthesized from sphingosine-1-phosphate (Avanti Polar Lipids) by acylation with palmitic anhydride (Sigma Aldrich) according to a protocol described in (65). The product was isolated by HPLC as described in (64), with an additional 1% NH_4OH in the eluent methanol. The product was positively identified by mass spectrometry and its purity verified by analytical HPLC. N-12Z-octadecenoyl-D-*erythro*-sphingosine (C18:1$^{\Delta 12c}$-cer) was synthesized from 12(Z)-octadecenoic acid (Larodan Fine Chemicals) and D-*erythro*-sphingosine (Sigma Aldrich), and N-stearoyl-D-*erythro*-sphinga-4E,14Z-diene (C18-sphingadiene-cer) from stearic acid (Sigma Aldrich) and D-*erythro*-sphinga-4E,14Z-diene (Avanti Polar Lipids) according to a protocol described in (65). The products were isolated by HPLC as described in (64), positively identified by mass spectrometry, and their purity verified by analytical HPLC. The lipids were dissolved as follows: POPC and C16-cer in methanol, Cer-1-P in methanol:water (100:1 by volume), C16-phyto-cer in choloform:methanol (1:1 by volume), and PSM, cholesterol, and all other ceramide analogs in hexane-isopropanol (3:2 by volume).

tPA was synthesized from methyl linolenate (Sigma Aldrich) as described in (66), isolated by HPLC, and positively identified by mass spectrometry. Purity of tPA was verified by analytical HPLC and absorbance and emission spectra (identical to published spectra). tPA was stored dry under argon at −87°C until dissolved in argon-purged methanol and used within a week. Cholesta5,7,9 (11)-trien-3-beta-ol (CTL) was synthesized and purified as described previously by Fischer and co-workers (67), stored dry under argon at −87°C until dissolved in ethanol and used within 10 days. 1-Palmitoyl-2-stearoyl-(7-doxyl)-*sn*-glycero-3-phosphocholine (7SLPC) was purchased from Avanti Polar Lipids, stored dry under argon at −87°C until dissolved in methanol and used within 5 months.

The water used for sample preparation was purified by reverse osmosis followed by passage through a UF-Plus water purification system (Millipore, Billerica, MA) to yield a product with final resistivity of 18.2 MΩcm.

DSC

Multilamellar vesicles (1 mM) for DSC were prepared by mixing equimolar amounts of PSM and the ceramide analogs, and evaporating the solvent under a stream of nitrogen. To remove any residual solvent, the lipid films were then kept under vacuum for 1 h. The dry lipid films were hydrated with argon-purged MQ-water in a water bath at 95°C for 1 h, followed by five cycles of freeze-thaw between liquid nitrogen and a 95°C water bath, interspersed with vigorous vortex mixing until opalescent and macroscopically homogeneous preparations were obtained. The samples were then cooled down to room temperature and degassed for 5 min with a ThermoVac instrument (MicroCal, Northampton, MA) before loading into the DSC. A total of 12 consecutive heating and cooling scans (1–90°C) operating with a 1°C/min temperature gradient were recorded with a high-sensitivity VP-DSC instrument (MicroCal) for two independently repeated samples. The presented thermograms were selected from the last heating cycles.

Steady-state fluorescence anisotropy

Multilamellar vesicles (37.5–50 μM total lipid; 75 to 100 nmol total lipid per 2 ml water) for fluorescence anisotropy measurements were prepared by mixing the lipids at the desired molar ratios (POPC/XCer, 60/15; POPC/PSM/XCer, 60/15/15; POPC/PSM/XCer/Chol, 60/15/15/10), and evaporating the solvent under a stream of nitrogen. Residual solvent was removed under vacuum for 1 h. The dry lipid films were then hydrated with argon-purged MQ-water in a water bath at 90°C for 60 min. Finally, the samples were vortex mixed and sonicated for 5 min in a water bath sonicator (FinnSonic M3 Bath Sonicator, FinnSonic Oy, Lahti, Finland) at 80°C. Immediately after sonication, tPA was added from a concentrated methanol stock solution to a final probe concentration of 1 mol %. Addition was done at constant stirring and no more than 0.2 volume % of methanol was added to any sample. The samples were cooled down to room temperature before the fluorescence measurements.

The steady-state fluorescence measurements were performed in quartz cuvettes on a PTI QuantaMaster-spectrofluorometer (Photon Technology International, Lawrenceville, NJ) operating in the T-format. The samples were kept under constant stirring and the temperature in the samples was controlled by a Peltier element with a temperature probe immersed in the sample. The fluorescence emission of tPA was scanned continuously at 405 nm (excitation 305 nm) while heating the samples at a rate of 2°C/min. The steady-state anisotropy, r, was determined as described in (68), by converting the fluorescence emission to anisotropy values with the PTI Felix32 software.

Time-resolved fluorescence measurements

Multilamellar vesicles (75–90 μM total lipid, 150 to 180 nmol total lipid per 2 ml water) for fluorescence lifetime measurements of tPA were prepared by mixing the lipids at the desired molar ratios (POPC/XCer, 60/15, POPC/PSM/XCer, 60/15/15, or POPC/PSM/XCer/Chol 60/15/15/10). The solvent was removed under a stream of nitrogen. The dry lipid films were then hydrated with argon-purged MQ-water in a water bath at 90°C for 60 min, followed by sonication for 5 min at 80°C. Immediately after sonication, 1 mol % tPA (2 nmol tPA) was added from a concentrated methanol stock solution. The samples were cooled down to room temperature before recording the fluorescence decays of tPA at 430 nm (excited with a 298-nm LED laser source) at 23°C and 10°C with a FluoTime 200-spectrofluorometer with a PicoHarp 300E time-correlated single photon counting module (PicoQuant, Berlin, Germany). The temperature was controlled by a Peltier element and the samples were kept under constant stirring. The data were analyzed with the FluoFit Pro software obtained from PicoQuant. The decay fits were obtained by a nonlinear least squares iterative reconvolution method, based on the Levenberg-Marquardt algorithm. The justification for the number of exponentials was assessed from the reduced χ^2 and a random distribution of the weighted residuals.

Fluorescence quenching assay

Fluorescence quenching measurements were performed by preparing two samples (50 μM total lipid) for each lipid mixture: the F-sample that in addition to the desired lipids contained both the quencher lipid (7SLPC) and the fluorescence reporter lipid (CTL), and the F_0-sample, which contained only the desired lipids and the reporter lipid CTL. The composition of the F-samples was thus POPC/7SLPC/PSM/XCer/Chol/CTL, 30/30/15/15/9/1 by mol, and the composition of the F_0-samples POPC/PSM/XCer/Chol/CTL, 60/15/15/9/1 by mol. After mixing the lipids, the solvent was removed under a stream of nitrogen followed by vacuum for 60 min. The dry lipid films were then stored under argon at −20°C until hydrated one at a time with argon-purged MQ-water at 65°C for 30 min. The samples were then sonicated in a water bath at 65°C for 5 min and cooled down to room temperature before the measurements. The fluorescence emission of CTL at 390 nm (excitation 324 nm) was registered continuously with a PTI QuantaMaster-spectrofluorometer, while heating the samples under constant stirring from 10 to 65°C at a rate of 5°C/min controlled by a Peltier element. Fluorescence quenching was calculated using the PTI Felix32 software and reported as the F/F0 ratio which denotes the fraction of unquenched fluorescence at a given temperature (63).

The method is based on collisional quenching between CTL and 7SLPC, which display different lateral partitioning in bilayers where sterol-rich domains and a disordered (POPC) bulk coexist. Thus, at low temperatures, the two molecules are physically separated, but as the temperature is increased and the sterol-rich domains subsequently become more disordered, the quenching susceptibility of CTL increases, allowing for the detection of temperature-induced melting of the sterol-rich domains. However, the absence of a detectable domain melting (i.e., efficient quenching of CTL fluorescence throughout the temperature interval under study) in bilayers in which highly ordered ceramide-rich domains coexist with a disordered bulk is indicative of the inability of CTL to partition into the ceramide-rich domains (55,63). Even though the total amount of 7SLPC is rather high, it apparently behaves similarly to POPC in the fluid phase, because domain melting in complex bilayers reported by SLPC and DSC has similar end-melting temperatures (55).

RESULTS AND DISCUSSION

Thermotropic properties of ceramide/PSM binary mixtures

The first part of this study was directed at determining the influence of structure on ceramide's interactions with PSM. The phase behavior of ceramide/PSM binary mixtures

(1:1) was studied with DSC (Fig. 1). In general, it can be stated that no apparent separation of the two sphingolipids into pure components occurred, but all of the ceramide molecular species interacted favorably with PSM, displaying more or less complex gel-to-fluid phase transitions originating from several constituent compositions. The midpoint temperatures (T_m) for the main gel-to-fluid transitions for the broad endothermic peaks are listed in Fig. 1.

Effect of saturated N*-acyl chain length*

The melting transition of the PSM/C16-cer binary mixture, with the main endotherm at slightly above 70°C (Fig. 1), agrees well with previous reports for this mixture (63,69-72). Reflecting the presence of several constituent compositions, this melting transition was previously deconvoluted into two components that differ in their relative ratios of the two sphingolipids (69). Introducing chain mismatch to the ceramides by increasing the *N*-acyl chain length from C16 to C18 or C24 gives very little variation in the T_m of the ceramides as pure components (ranging from 91°C to 93°C (9,45)). Similarly, variation in the *N*-acyl chain length resulted in rather small differences in the main T_m when the ceramides were mixed with PSM (Fig. 1). A slightly lower T_m was observed in the presence of C18-cer and C24-cer compared to C16-cer (Fig. 1), even though C16-cer displays the lowest T_m of these ceramides as a pure component. However, increasing the degree of chain asymmetry appeared to result in an increase in the complexity of the transition (broadening of the transition peak). This was probably a result of larger hydrophobic mismatch leading to lower molecular packing and a lower degree of interactions, which has been observed in monolayer studies with various binary mixtures of SMs and ceramides with different *N*-acyl chain lengths (46).The particularly complex and broad transition recorded for the C24-cer/PSM mixture was probably also in part attributable to chain interdigitation.

Effect of interfacial hydroxyls and phosphate headgroup

In general, SMs and ceramides containing a phytosphingosine backbone display higher gel-to-fluid transition temperatures (as pure components) than analogous sphingolipids with a sphingosine backbone (47,73). For example, C18-phyto-cer melts at 110°C (48), whereas C18-cer melts at 91–93°C (9,45). This observation is attributable to an enhanced H-bonding capacity due to the additional C4-OH of the phytosphingosine backbone. However, according to both monolayer (74) and infrared studies (47), phytosphingosine chains pack less tightly than sphingosine chains. This likely explains the observation in Fig. 1, in which the C16-phyto-cer/PSM mixture displays a ~4°C lower transition temperature relative to the C16-cer/PSM mixture. Thus, it appears that when C16-phyto-cer is mixed with PSM the destabilizing effect of the looser chain packing of C16-phyto-cer becomes more pronounced than the stabilizing effect of an enhanced H-bonding capacity.

Similar to the hydroxyl in phytosphingosine, an α-hydroxylation (C2-OH) of the *N*-acyl chain is reported to cause an increase in the T_m of pure SM relative to

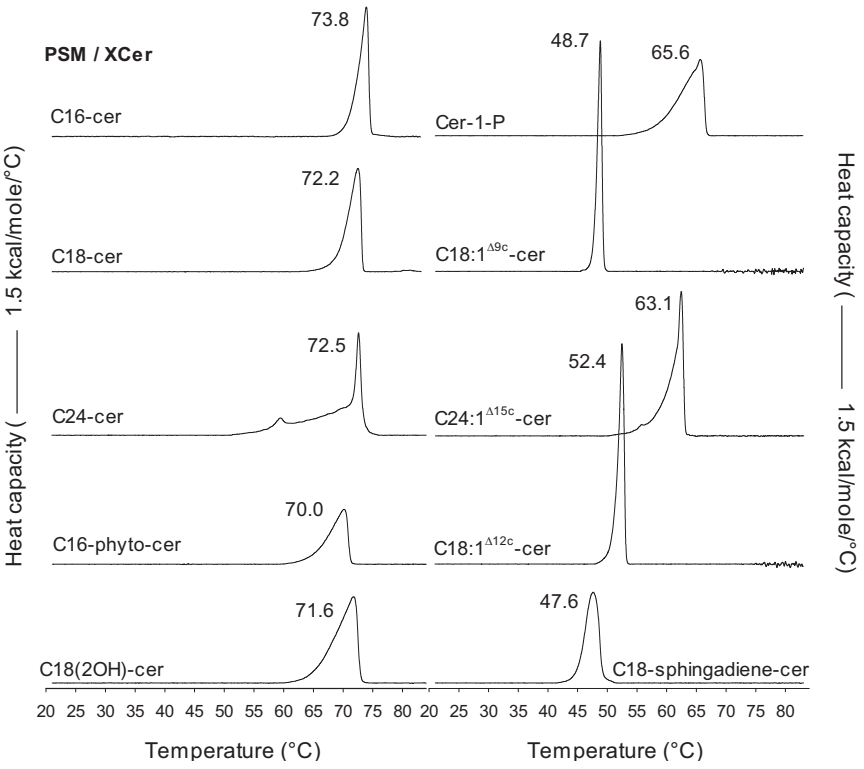

FIGURE 1 DSC thermograms of binary ceramide-PSM bilayers. Representative thermograms of the 6th heating scans (1°C/min) of equimolar binary mixtures (1 mM) of the ceramides and PSM from two independently repeated experiments are shown. The T_m for the main (*highest*) transition peak is given for each mixture.

nonhydroxylated SM (75). An α-hydroxylation also stabilizes the molecular packing of ceramides relative to their nonhydroxylated counterparts (76). However, in this study, the T_m for the binary mixtures with PSM was nearly equal (<1°C difference) for both C18(2OH)-cer and the chain equivalent C18-cer (Fig. 1), indicating that in a binary mixture of an α-hydroxylated ceramide and a nonhydroxylated SM, the stabilization of intermolecular interactions by the α-hydroxylation was no longer apparent. Interestingly, both in phytoSM and phytoceramide, introduction of an α-hydroxylation causes a clear reduction in the T_m and destabilization of chain interactions (47,48,73), possibly due to weakening of the amide H-bonding (47) together with suggested sterical hindrance for acyl chain packing (48) induced by the α-hydroxylation. These observations indicate that specific physical properties mediated by a structural detail, such as the α-hydroxylation-induced stabilization of the interlipid interactions of sphingolipids with sphingosine backbone, do not necessarily become transferred as such into other, closely related sphingolipid species, or into mixtures of several sphingolipid species.

Due to the highly polar phosphate headgroup, Cer-1-P displays very different biophysical properties from those of ceramide. In contrast to ceramide, the molecular structure of Cer-1-P allows it to form bilayers in aqueous media when present as a pure component (49). Cer-1-P in its pure state also displays a significantly lower gel-to-fluid transition temperature (~65°C (49)) relative to the chain-matched C16-cer (~90°C (77,78)). This is a consequence of headgroup repulsion within Cer-1-P, and the subsequent reduction in its lateral chain packing. Thus, it was not unexpected that the T_m for the binary mixture of PSM with Cer-1-P was significantly lower than with the chain equivalent C16-cer, displaying also a broader transition peak indicating complex gel phase transition and poor miscibility with PSM (Fig. 1). Interestingly, the end-melting of the main phase transition of the Cer-1-P/PSM mixture, which did not display any apparent separation of PSM and Cer-1-P into pure components, appeared almost at an equal temperature as the transition for pure Cer-1-P.

Effect of unsaturated N*-acyl chain and long-chain base*

Cis-double bonds in lipid acyl chains perturb the chain packing, reducing the chain order and subsequently, also the gel-to-fluid transition temperature of lipids in a position-dependent way (79). Thus, it is not surprising that both C18:1$^{\Delta 9c}$-cer and C24:1$^{\Delta 15c}$-cer in binary mixtures with PSM displayed lower T_ms than their saturated counterparts (Fig. 1). A larger reduction in the T_m was induced by the double bond in C18:1$^{\Delta 9c}$-cer (~23°C lower than C18-cer) than in C24:1$^{\Delta 15c}$-cer (~9°C lower than C24-cer), which reflects the position-dependent effect of *cis*-unsaturations on the chain packing. In both C18:1$^{\Delta 9c}$-cer and C24:1$^{\Delta 15c}$-cer, the *cis*-double bond increases the lateral space requirement of the molecules, but the effect is clearly more pronounced in C18:1$^{\Delta 9c}$-cer in which the double bond is located in the middle region of the *N*-acyl chain, as opposed to the double bond in C24:1$^{\Delta 15c}$-cer, which is located closer to the membrane hydrophobic core, next to the distal end of the sphingoid base where the disruption in chain packing is less dramatic (74). Accordingly, the *cis*-double bond in C18:1$^{\Delta 12c}$-cer also caused a reduction in the T_m of the binary mixture relative to C18-cer, but the magnitude of this effect was somewhat smaller than for C18:1$^{\Delta 9c}$-cer. Altogether, the transitions of the binary mixtures of PSM with the ceramides having unsaturated *N*-acyl chains appeared much more cooperative than the transitions for mixtures containing saturated or hydroxylated ceramides, indicating higher miscibility for the former.

Interestingly, compared to the saturated C18-cer, the *cis*-double bond in the sphingoid base of C18-sphingadiene-cer appeared to induce a larger reduction in the T_m of the binary mixture than the *cis*-double bond in the approximately corresponding bilayer depth in C18:1$^{\Delta 12c}$-cer (refer to Scheme S1 for the chemical structures). Furthermore, the melting transition of the C18-sphingadiene-cer/PSM mixture was clearly less cooperative than the transition of the C18:1$^{\Delta 12c}$-cer/PSM mixture. These results indicate that the unsaturation in the *N*-acyl chain disturbed the ceramide/PSM interactions to a lesser degree than the unsaturation in the sphingoid base, suggesting a difference between the ceramide hydrocarbon chains in their interactions with PSM, perhaps because of the different effects of the double bonds on the interfacial region of ceramide. The *cis*-double bond in the sphingoid base is likely to induce orientational disorder about the C4 *trans*-double bond, which is an important factor in promoting close packing of ceramide acyl chains (74,80), and has been suggested as having a role in the stabilization of the intermolecular network of H-bonds within ceramides (80,81).

Properties of the ceramides in fluid POPC bilayers

Next, we studied the properties of the ceramides in binary mixtures with POPC, ternary mixtures with POPC and PSM, as well as in quaternary mixtures with POPC, PSM, and cholesterol. The formation and thermal stability of ceramide(/PSM)-rich domains in POPC was determined from the anisotropy of tPA in the bilayers as a function of increasing temperature (Fig. S1). In POPC bilayers that contain C16-cer (at the molar fraction used in this study), ceramide is known to laterally segregate into highly ordered ceramide-rich domains that coexist with a ceramide-poor POPC-rich fluid phase (16). In such bilayers, tPA will partition preferably into the ordered ceramide-rich phase (15,17,51,53), and in the low temperature range display high anisotropy values indicative of high molecular order. Upon increasing the temperature the anisotropy decreases as the domains melt, until finally reaching a point where it levels off to values typical for a fluid bilayer

(Figs. S1–S3). In this study, we refer to the end-melting of the ordered domains (as determined by tPA anisotropy measurements), and list the temperatures for different compositions in Table 2.

In addition to steady-state anisotropy, we also measured the time-resolved fluorescence decays of tPA in these mixtures to further explore the properties of the domains formed by the ceramides. The excited-state lifetime of tPA is sensitive to the packing order in its surroundings, becoming significantly longer in ordered phases than in fluid phases (15,51,82,83). The tPA lifetimes, therefore, provide a sensitive means of deducing heterogeneities in the degree of lateral chain packing within bilayer membranes, especially in the context of ceramide-rich phases. However, one should keep in mind that tPA lifetime components are dependent on the lateral partitioning of tPA in various environments, and this partitioning behavior can differ as the compositon of the bilayers varies. It is unfeasible to determine partition-coefficients for tPA in all possible phases and the compositions used; therefore, tPA lifetime data for different systems should be compared with some caution. The mean fluorescence lifetime, which is calculated based on the fractional contributions of all the lifetime components present in a given system, together with the longest lifetime components attributable to the most ordered phases (i.e., the ceramide-rich domains) present in the bilayers, are shown in Figs. 2 and 3, whereas all individual decay components are listed in Tables S1–S4.

Saturated ceramides in POPC bilayers

Although the saturated C16-, C18-, and C24-cer display little variation in their T_m as pure components (ranging from 91°C to 93°C (9,45)), and in binary mixtures with PSM (ranging from 72.2 to 73.8°C, Fig. 1), their domain melting temperatures in POPC bilayers were observed to increase with regard to the *N*-acyl chain length (Table 2, *binary mixtures*). This observation is in line with previously reported results for comparable mixtures with POPC (14). However, very little variation was observed both in the average fluorescence lifetime and the longest lifetime component of tPA (attributable to the ceramide-rich domain) in these bilayers at 23°C (Fig. 2 *A*). This indicates that, although the thermal stability of the ceramide-rich domains in POPC was affected by the *N*-acyl chain length, the average degree of acyl chain packing in the bilayers and the degree of packing within the ceramide-rich domains were nearly unaffected. In the presence of PSM, the saturated Cer domains in POPC melted between 47°C and 49°C (Table 2). This higher temperature is in part due to an increase in the amount of ordered lipids relative to the fluid POPC.

Hydroxylated ceramides and Cer-1-P in POPC bilayers

The sphingosine-based C16-cer and the chain equivalent C16-phyto-cer displayed rather similar domain melting temperatures in POPC bilayers both in the absence and presence of PSM (Table 2), indicating that the thermal stability of the domains was not affected by the additional hydroxyl in C16-phyto-cer, although it reduced the transition temperature of ceramide/PSM mixtures (Fig. 1). However, a clear decrease in the average degree of bilayer order and the packing order of the ceramide-rich domains was observed for C16-phyto-cer relative to C16-cer, both in the absence and presence of PSM (Fig. 2 *A*). This could be related to the less tight packing of phytosphingosine chains observed previously (47,74). However, PSM appeared to be able to increase the packing order in the C16-phyto-cer containing bilayers both in general (tPA average lifetime) and within the ordered domains (*longest lifetime component*, Fig. 2 *C*). Interestingly, phytoceramide was previously found to stabilize lateral domains relative to C16-cer (43). The use of different fluorescent probes to detect the melting of ordered domains (long-chain TMA-DPH (43) versus tPA), and possible compositional differences could explain the observed difference. On the other hand, in SM, a phytosphingosine backbone appears to induce thermal stabilization both in the pure state as well as in mixtures (73).

TABLE 2 Melting temperatures for ceramide-rich domains in various mixed bilayers

XCer	POPC/XCer (60:15)	POPC/PSM/XCer (60:15:15)	POPC/PSM/XCer/CHOL (60:15:15:10)
C16-cer	41.5 ± 0.7	47.1 ± 0.2	44.3 ± 1.0
C18-cer	42.9 ± 1.2	48.2 ± 0.3	44.3 ± 0.8
C24-cer	46.2 ± 1.0	49.0 ± 0.6	44.0 ± 0.3
C16-phyto-cer	42.0 ± 1.4	47.1 ± 0.5	41.2 ± 1.3
C18(2OH)-cer	44.7 ± 0.3	49.3 ± 0.3	45.5 ± 0.1
Cer-1-P	39.0 ± 1.4	45.0 ± 0.6	40.4 ± 0.1
C18:1$^{\Delta 9c}$-cer	16.1 ± 1.2	24.1 ± 0.2	~19.5 ± 0.3[a]
C24:1$^{\Delta 15c}$-cer	28.7 ± 0.3	38.4 ± 0.1	31.4 ± 0.2
C18:1$^{\Delta 12c}$-cer	19.8 ± 0.3	31.0 ± 0.7	~23.7 ± 0.4[a]
C18-sphingadiene-cer	16.6 ± 0.1	24.6 ± 0.9	~26.8 ± 0.3[a]

The values were deduced from two to three independently repeated measurements of tPA (1 mol %) fluorescence anisotropy as a function of increasing temperature.

[a]The values listed for the quaternary mixture bilayers in the presence of the C18-unsaturated molecular species are based on the most accurate approximations that we were able to conduct based on the raw data, because the anisotropies for these bilayers did not clearly level off at a certain temperature in these mixtures.

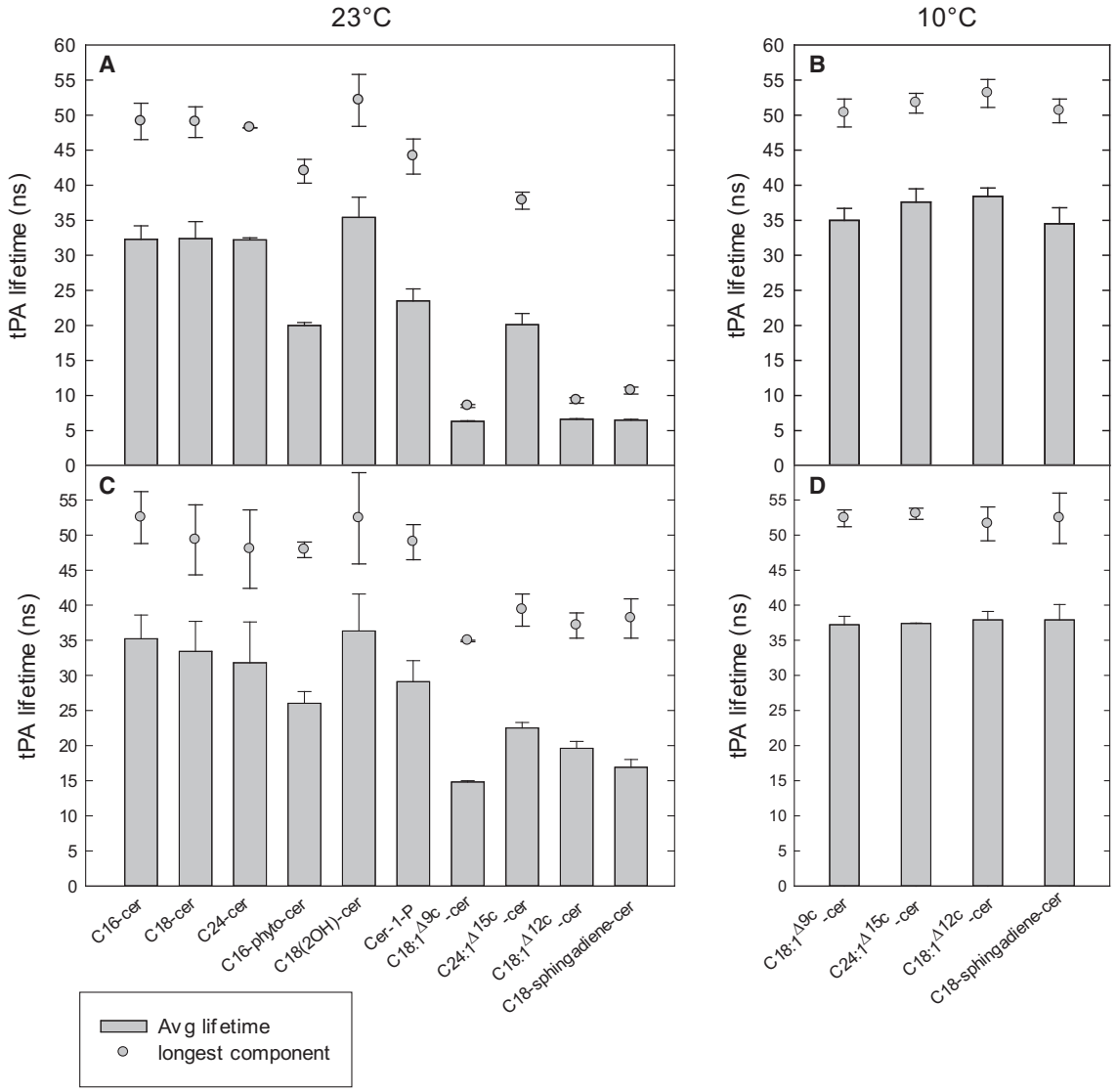

FIGURE 2 Fluorescence lifetimes of tPA in various mixed bilayers. The average lifetime of tPA (1 mol %) in binary (POPC/XCer 60:15, *A* and *B*) and ternary (POPC/PSM/XCer 60:15:15, *C* and *D*) mixture bilayers was measured at 23°C (*A* and *C*) and 10°C (*panels B* and *D*). The longest lifetime components of tPA (signifying the most ordered phase) are given for each mixed bilayer as a solid circle above each bar. Each value is the average from at least three independently repeated experiments. For complete tables of all lifetime components in the various mixtures see Tables S1 and S2.

The additional hydroxyl in C18(2OH)-cer again appeared to slightly increase both the domain melting temperature (Table 2) and the degree of chain packing in the bilayers (Fig. 2, *A–C*), relative to the chain-matched C18-cer both in the presence and absence of PSM. Similar stabilization of interlipid interactions by α-hydroxylation of the *N*-acyl chain has been reported for SM (73). The effect of PSM on the bilayer properties of C18(2OH)-cer were similar to those observed for the saturated *N*-acyl chain variants, with a clear thermal stabilization induced by increased fraction of ordered lipids (Table 2), but no apparent effect on the average degree of bilayer order or order within the domains (Fig. 2 *C*).

Given that Cer-1-P displays significantly lower T_m as a pure component (~65°C (49)) than many ceramides (~90°C or above), perhaps an unexpectedly high domain melting temperature was observed for Cer-1-P in the POPC bilayers both in the absence and presence of PSM (Table 2), being only a few degrees lower than for the chain-equivalent C16-cer. Together with the observed lateral segregation of Cer-1-P (and Cer-1-P together with PSM) into high-melting temperature domains in our experiments, this suggests that in mixed bilayers Cer-1-P displays a behavior similar to ceramides, although DSC and NMR studies have shown that the two-phase coexistence in Cer-1-P/PC mixtures is limited to a narrower temperature range than in C16-cer/PC mixtures, and that PC bilayers are significantly less perturbed by Cer-1-P than by C16-cer (50). Thus, although similar thermal stabilities in POPC bilayers are displayed (Table 2), the differences in

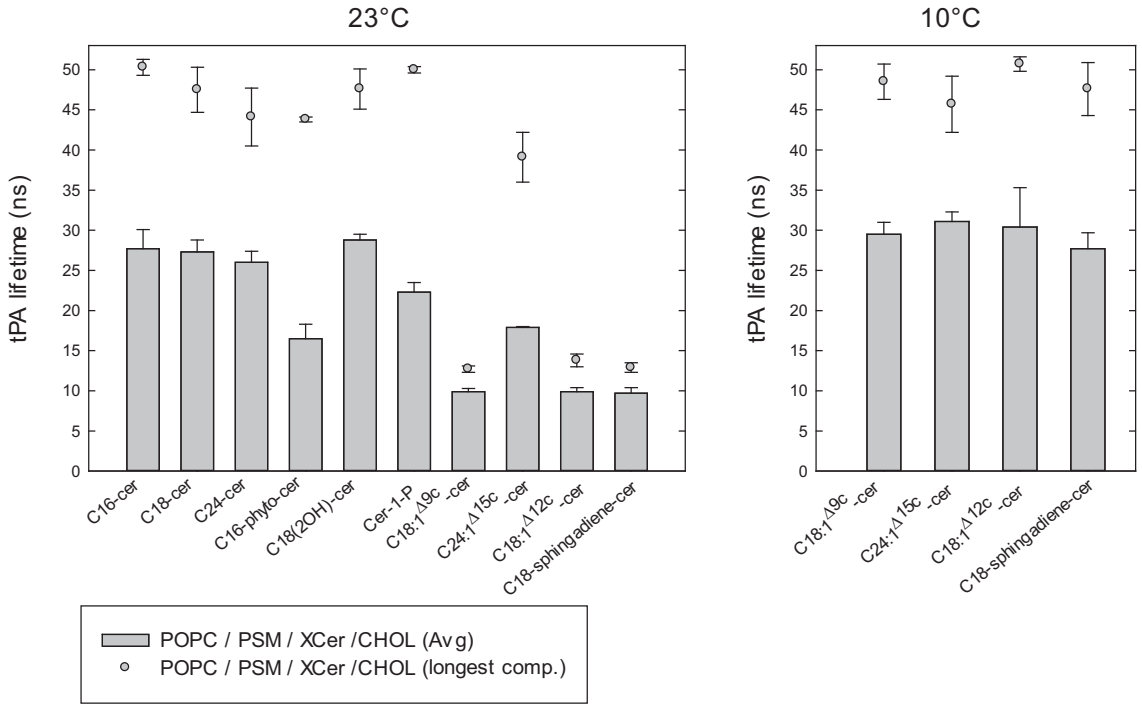

FIGURE 3 Fluorescence lifetimes of tPA in quaternary mixed bilayers. The average lifetime of tPA (1 mol %) in the mixed bilayer (POPC/PSM/XCer/Chol 60:15:15:10) was measured at 23°C (*left panel*) and 10°C (*right panel*). The longest lifetime components of tPA (signifying the most ordered phase) are given for each composition as a solid circle above each bar. Each value is the average from at least three independently repeated experiments. For complete tables of all lifetime components, see Tables S3 and S4.

bilayer properties between these two ceramides becomes apparent in the significantly lower degree of average bilayer packing order and the packing order within the ceramide-rich domains in the presence of Cer-1-P relative to C16-cer both in the absence and presence of PSM (Fig. 2, *A–C*). The phosphate headgroup clearly limited the chain interactions in Cer-1-P relative to C16-cer, resulting in decreased lateral packing and (slightly) reduced thermal stability.

Unsaturated ceramides in POPC bilayers

All the unsaturated ceramides appeared capable of forming laterally segregated domains with apparent domain melting in POPC bilayers (Fig. S1). However, as could be expected from the reduced lateral packing of unsaturated acyl chains that destabilize chain interactions, the domain melting temperatures for the unsaturated ceramides were significantly lower than for the other ceramides (Table 2). A similar effect of *cis*-unsaturations on the thermally induced melting of C18- and C24-cer domains in POPC bilayers was previously reported (14). Within the unsaturated molecular species studied here, the most thermally stable were the C24:$1^{\Delta 15c}$-cer-rich domains, followed by the C18:$1^{\Delta 12c}$-cer- and the C18:$1^{\Delta 9c}$-cer-rich domains. This sequence, which also applied in the ternary mixtures with PSM, reflects the position-dependent effect of unsaturations on acyl chain packing, which was also apparent in the DSC experiment (Fig. 1). Similar positional effects of disturbed chain packing on the thermal stability of ceramide-rich domains have also been observed for methyl-branched ceramides, with a branch in the middle region of the *N*-acyl chain having a greater destabilizing effect than branches closer to the distal end of the chain (84). A comparison of the binary bilayers of POPC and C18-sphingadiene-cer or C18:$1^{\Delta 12c}$-cer reveals that the unsaturation of the sphingoid base resulted in a lower domain melting temperature relative to the unsaturation of the *N*-acyl chain (Table 2), in a similar way as the unsaturation of the sphingoid base was observed to destabilize the ceramide-PSM interactions to a greater degree (Fig. 1).

The tPA lifetimes measured in the binary POPC bilayers that contained unsaturated ceramides revealed that only C24:$1^{\Delta 15c}$-cer was able to form a well-ordered environment at 23°C, whereas all other mixtures displayed a significantly lower average and the longest lifetimes, which reflected a fluid state for the bilayers (Fig. 2 *A*). This observation agreed well with the anisotropy data showing that for the bilayers that contained C24:$1^{\Delta 15c}$-cer, a fraction of an ordered phase still existed at 23°C (the melting occurring well above this temperature), whereas the domains formed by the rest of the unsaturated species had already melted (Table 2, Fig. S1). PSM, however, seemed capable of increasing the chain order in these bilayers (especially relative to C24:$1^{\Delta 15c}$-cer, Fig. 2 *C*), allowing for the observation of

longer lifetime components and an increase in the average degree of bilayer order.

The emission decays of tPA for the bilayers that contained unsaturated ceramides were also measured at 10°C, a temperature at which, according to the tPA-anisotropy data (Fig. S1), highly ordered phases enriched in the unsaturated ceramides were present. The tPA lifetimes obtained at 10°C clearly showed that the average degree of bilayer order increased relative to the measurements performed at 23°C, with each of the unsaturated ceramides forming a highly ordered ceramide-rich phase (Fig. 2 *B*).Very little variation between the different mixtures occurred, indicating similar degrees of chain packing in the bilayers irrespective of the double bonds or the presence of PSM (Fig. 2 *D*).

The effects of cholesterol and ceramides on domain formation

Like ceramide, cholesterol also interacts favorably with saturated SMs, resulting in the formation of SM/cholesterol-rich ordered phases (85,86). As they appear to share the willingness to interact with SM, the coexistence of ceramide and cholesterol in a bilayer may lead to a situation in which they compete over interactions with SM. The subsequent influences that ceramides and cholesterol have on each other in bilayer membranes are complex and highly dependent on the membrane composition, with two main phenomena identified: a ceramide-induced displacement of cholesterol from ordered (e.g., SM-rich) phases (18,54,55) and a cholesterol-induced destabilization and solubilization of ceramide-rich phases (51,53,57,59). In general, the former predominates at low cholesterol levels, whereas the latter is effective at high cholesterol levels. Furthermore, in the absence of a fluid phase, SM, cholesterol, and ceramide may coexist to form a ternary phase (58,87). Nevertheless, within certain circumstances ceramide is known to effectively displace cholesterol from ordered lipid domains, which we have demonstrated previously with the use of the CTL-quenching method in mixed POPC/PSM/cholesterol/ceramide bilayers. With this method, the absence of a detectable melting of a CTL-rich domain signifies displacement of the cholesterol-mimicking probe from the domains into the fluid POPC-rich phase where it becomes effectively quenched by the fluid quencher lipid (55,63).

Saturated ceramides and cholesterol

In the presence of cholesterol, the saturated ceramides (C16-, C18-, and C24-cer) showed domain end-meltings around 44°C (Table 2). At 23°C, these domains had rather similar lateral packing properties, as revealed by tPA average lifetime (Fig. 3, *left panel*), although the longest lifetime component of tPA indicated some domain disorder by the increased acyl chain mismatch (Fig. 3, *left panel*). Even though cholesterol was present in the bilayer, it is unlikely that it was incorporated into the ceramide-rich domains, as no sterol-rich domain melting could be observed in these bilayers (Fig. 4 *A*). In the absence of saturated ceramide, a sterol-enriched PSM domain would show an end-melting slightly below 40°C (at the 60:30:10 POPC/PSM/Chol composition (55,63)).

Next, we examined whether hydroxylated ceramides and Cer-1-P could exclude cholesterol from the ceramide-rich ordered domains (Fig. 4 *B*). The CTL-quenching assay clearly showed that cholesterol affected these bilayers differently depending on the structure of the ceramide. Although the presence of C18(2OH)-cer caused an efficient displacement of cholesterol from the ceramide-rich domain, C16-phyto-cer apparently failed to displace cholesterol (as suggested by CTL's relative protection from quenching below 35°C. In the presence of Cer-1-P, a gradual decrease of F/F_0 was apparent over the temperature range of 10–40°C, with no evidence of an abrupt sterol-enriched domain melting (Fig. 4 *B*). Thus, it appeared that in the presence of C18(2OH)-cer, cholesterol was to a large extent displaced from the ordered domains, although in the presence of Cer-1-P and C16-phyto-cer, it was incorporated to a small or a large extent into the ceramide-rich domains. We cannot rule out the possibility that cholesterol could actually displace C16-phyto-cer from the PSM-rich domains.

Unsaturated ceramides and cholesterol

Determining the melting temperature for domains formed in the quaternary mixture bilayers that contained unsaturated ceramides from the tPA-anisotropy data was not straight forward in all cases, because the anisotropies in those bilayers did not always clearly level off at a certain temperature (Fig. S3). Thus, the domain melting temperatures listed for the quaternary mixture bilayers in the presence of the C18-unsaturated molecular species in Table 2 are based on the most accurate approximations that we were able to conduct based on the raw data. C24:$1^{\Delta 15c}$-cer/PSM-rich domains displayed the highest end-melting temperature (Table 2), and also the highest average tPA lifetime of the unsaturated ceramides examined at 23°C (Fig. 3, *left panel*). For the other unsaturated ceramides, both the average and longest lifetimes were similar to each other, and only deviated from C24:$1^{\Delta 15c}$-cer at 23°C. At 10°C, all the unsaturated ceramides had very similar lifetime values, both in pure POPC (Fig. 2 *B*), in POPC together with PSM (Fig. 2 *D*), and also when cholesterol was included in the quaternary mixed bilayers (Fig. 3, *right panel*). Apparently, at the lower temperature, the ceramide domain order approached that of C24:$1^{\Delta 15c}$-cer in all tested systems. CTL-quenching data (Fig. 4 *C*) also suggested that C24:$1^{\Delta 15c}$-cer was able to exclude cholesterol from the ordered domains. In the presence of the C18-unsaturated ceramides a clear domain melting could be observed with the CTL-quenching assay (Fig. 4 *C*), demonstrating that cholesterol was incorporated into the ordered domains of

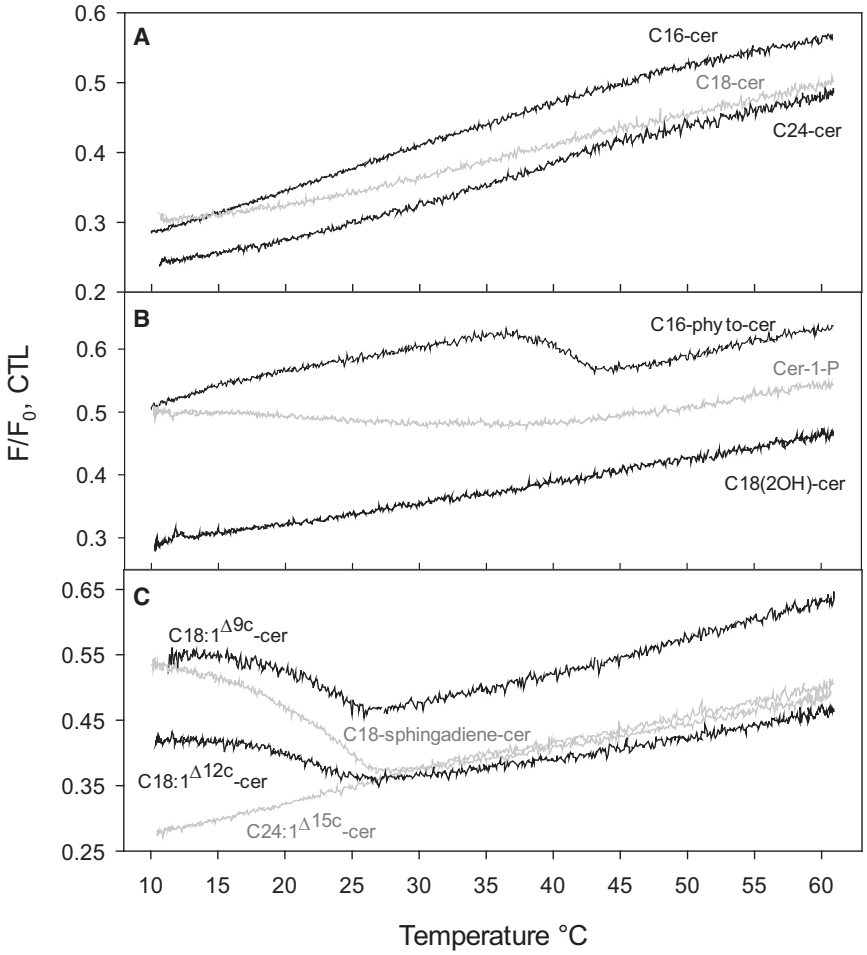

FIGURE 4 Quenching of CTL fluorescence in quaternary mixture bilayers containing the ceramides with varying acyl chain length (*A*), interfacial hydroxyl groups or phosphate headgroup (*B*), and unsaturated chains (*C*). The 7SLPC-induced quenching of CTL fluorescence was measured in the F-samples (7SLPC/POPC/PSM/XCer/Chol/CTL; 30/30/15/15/9/1 by mol) and the F_0-samples (POPC/PSM/XCer/Chol/CTL; 60/15/15/9/1 by mol). F/F_0 thus denotes the fraction of unquenched CTL fluorescence as a function of increasing temperature. Representative quenching curves from at least three independently repeated experiments are shown for each mixture.

these bilayers. The fraction of CTL that was initially shielded from quenching (at a low temperature range) appeared higher for both C18-sphingadiene-cer and C18:1$^{\Delta 9c}$-cer, than for C18:1$^{\Delta 12c}$-cer (higher values of F/F_0), which we interpret as a sign of more cholesterol being incorporated into the domains in the presence of the two first mentioned. The presence of cholesterol in the PSM-rich domains was further supported by data for the longest lifetime component of tPA, which decreased significantly in the cholesterol-containing bilayers (Fig. 3, *left panel*) compared to cholesterol-free ternary compositions (Fig. 2 *C*) suggesting a lower degree of order by inclusion of cholesterol.

CONCLUSIONS

The results in the current study clearly demonstrate that in fluid POPC bilayers, saturated and hydroxylated ceramide species form domains with significantly higher degrees of chain packing and thermal stability than unsaturated species. Furthermore, saturated and hydroxylated ceramide species formed gel phases of higher transition temperatures than the unsaturated ceramide species in binary mixtures with PSM. These observations indicate that the ordering in the acyl chain region, which is significantly reduced by unsaturation, is a major factor influencing the interactions of different molecular species of ceramides with PSM. Similar conclusions were previously drawn based on monolayer studies with various ceramide-SM mixtures, which revealed that the phase behavior of mixtures of these two sphingolipids was ultimately determined by the acyl chain order (46). Furthermore, we found that all of the ceramide molecular species interacted favorably with PSM, indicating that ceramides, despite differences in the chemical structures between different molecular species, display an inherent affinity for ordered (saturated) lipids. This conclusion is in agreement with the observation that ceramides display a uniquely high affinity for ordered domains (88). The ordering of the acyl chain region appears to be of direct functional importance, as solid-like ceramides typically occur in the skin and are important for maintaining its barrier functions, whereas unsaturated species occur in membranes where less solid properties are needed, such as in brain tissue.

Our results also reveal that the differences in bilayer properties within different saturated species of ceramides, for which the presence of interfacial hydroxyl groups or the

length of the *N*-acyl chain varies, are smaller than differences within different unsaturated species. Similar observations were presented in a previous report, in which the effect of ceramide acyl chain length and unsaturation on membrane biophysical properties was studied (14). We propose that the length of the *N*-acyl chain, as well as the presence of interfacial hydroxyls, cause relatively small variations in the bilayer properties of ceramides, perhaps providing merely fine adjustments in the interactions of ceramides with coexisting lipids.

Our current results, when viewed against previous observations on different ceramide molecular species, indicate that the bilayer behavior of ceramides is not always easily deduced from their molecular structure. For example, the additional hydroxyl in phytoceramide stabilizes this lipid in its pure state (47), whereas our results show a slight destabilization of its interlipid interactions in mixed bilayers relative to the sphingosine-based ceramide. Interestingly, C16-phyto-cer failed to markedly displace cholesterol from the ceramide-rich domains, in sharp contrast to the effects of C16-cer. The interfacial region of C16-phyto-cer is more polar than C16-cer, and therefore its affinity to PSM may be smaller than that of cholesterol. A consequence of this could be that cholesterol in fact displaces C16-phyto-cer from the PSM-rich domain. However, our current data do not allow us to verify this suggestion.

It should be noted that Cer-1-P has been suggested not to segregate into lateral lipid domains in PC bilayers (50), but our results suggest that in certain mixtures, Cer-1-P appears to be able to form domains that are relatively stable and ordered. Interestingly, specific structural details may not equally influence closely related sphingolipid species, as exemplified by a stabilization of the interactions of sphingosine-based ceramides (76) and SMs (75) by α-hydroxylation of their *N*-acyl chains as opposed to a destabilization induced by such a hydroxylation of phytosphingosine-based ceramides (48) and SMs (73).

Our results also demonstrate that the relative position of *cis*-double bonds in unsaturated ceramide species has a significant impact on the biophysical properties of the bilayers, with a destabilizing effect that appears to be stronger the closer the double bond is located to the midpart of the *N*-acyl chain. A position-dependent effect of unsaturations on the lipid acyl chain packing is evident also in glycerophospholipids (79), and has been explained by a maximum decrease in van der Waal's interactions between lipid acyl chains when one of them is separated into two equally long segments by a double bond (89). We have reported similar effects on acyl chain packing by methyl-branched acyl chains (84) which are common in the ceramides of aquatic organisms. Thus, unsaturation and methyl-branches in ceramides of distinct organisms probably serve a similar function of rendering the ceramides a more fluid nature. As a double bond in the sphingoid base was found to influence the interlipid interactions of ceramides somewhat differently than a double bond in the *N*-acyl chain, ceramides with unsaturated sphingoid bases increase the repertoire of ceramide molecular species with possible distinct biological functions.

In conclusion, it is clear that the chemical nature affects the interactions of ceramides with other lipid species, with the overall membrane composition also having an impact on the ultimate biophysical properties of membranes that contain ceramides. Different ceramide molecular species, which are needed to meet the functional requirements of each type of biological membrane or tissue, are expected to affect the properties of membranes in numerous ways. Although it is clear that saturated and hydroxylated ceramide species, even at physiological temperatures, may exist in highly ordered conformations, unsaturated species are more fluid in nature.

SUPPORTING MATERIAL

One scheme, three figures, and four tables are available at http://www.biophysj.org/biophysj/supplemental/S0006-3495(15)00922-4.

AUTHOR CONTRIBUTIONS

The authors contributed as follows: T.M. and J.P.S. conceived the study. Md.A.A.S. and T.M. performed the experiments and data analysis. T.M. wrote the article with contributions from Md.A.A.S. and J.P.S.

ACKNOWLEDGMENTS

We thank Peik Ekman for help with some of the fluorescence lifetime measurements.

The study was funded by generous grants from the Sigrid Juselius Foundation, the Academy of Finland, and the Åbo Akademi Foundation.

REFERENCES

1. Levy, M., and A. H. Futerman. 2010. Mammalian ceramide synthases. *IUBMB Life.* 62:347–356.
2. Laviad, E. L., L. Albee, …, A. H. Futerman. 2008. Characterization of ceramide synthase 2: tissue distribution, substrate specificity, and inhibition by sphingosine 1-phosphate. *J. Biol. Chem.* 283:5677–5684.
3. Mathias, S., L. A. Peña, and R. N. Kolesnick. 1998. Signal transduction of stress via ceramide. *Biochem. J.* 335:465–480.
4. Pushkareva, M., L. M. Obeid, and Y. A. Hannun. 1995. Ceramide: an endogenous regulator of apoptosis and growth suppression. *Immunol. Today.* 16:294–297.
5. Hannun, Y. A., and C. Luberto. 2000. Ceramide in the eukaryotic stress response. *Trends Cell Biol.* 10:73–80.
6. Futerman, A. H. 2002. Ceramide Signaling. Kluwer Academic/Plenum Publishers, New York, USA.
7. Bartke, N., and Y. A. Hannun. 2009. Bioactive sphingolipids: metabolism and function. *J. Lipid Res.* 50 (*Suppl*):S91–S96.
8. Stancevic, B., and R. Kolesnick. 2010. Ceramide-rich platforms in transmembrane signaling. *FEBS Lett.* 584:1728–1740.
9. Westerlund, B., P. M. Grandell, …, J. P. Slotte. 2010. Ceramide acyl chain length markedly influences miscibility with palmitoyl sphingomyelin in bilayer membranes. *Eur. Biophys. J.* 39:1117–1128.

10. Holopainen, J. M., J. Lemmich, …, P. K. Kinnunen. 2000. Dimyristoylphosphatidylcholine/C16:0-ceramide binary liposomes studied by differential scanning calorimetry and wide- and small-angle x-ray scattering. *Biophys. J.* 78:2459–2469.
11. Huang, H. W., E. M. Goldberg, and R. Zidovetzki. 1996. Ceramide induces structural defects into phosphatidylcholine bilayers and activates phospholipase A2. *Biochem. Biophys. Res. Commun.* 220:834–838.
12. Holopainen, J. M., J. Y. Lehtonen, and P. K. Kinnunen. 1997. Lipid microdomains in dimyristoylphosphatidylcholine-ceramide liposomes. *Chem. Phys. Lipids.* 88:1–13.
13. Holopainen, J. M., M. Subramanian, and P. K. Kinnunen. 1998. Sphingomyelinase induces lipid microdomain formation in a fluid phosphatidylcholine/sphingomyelin membrane. *Biochemistry.* 37:17562–17570.
14. Pinto, S. N., L. C. Silva, …, M. Prieto. 2011. Effect of ceramide structure on membrane biophysical properties: the role of acyl chain length and unsaturation. *Biochim. Biophys. Acta.* 1808:2753–2760.
15. Silva, L., R. F. de Almeida, …, M. Prieto. 2006. Ceramide-platform formation and -induced biophysical changes in a fluid phospholipid membrane. *Mol. Membr. Biol.* 23:137–148.
16. Hsueh, Y. W., R. Giles, …, J. Thewalt. 2002. The effect of ceramide on phosphatidylcholine membranes: a deuterium NMR study. *Biophys. J.* 82:3089–3095.
17. Castro, B. M., R. F. de Almeida, …, M. Prieto. 2007. Formation of ceramide/sphingomyelin gel domains in the presence of an unsaturated phospholipid: a quantitative multiprobe approach. *Biophys. J.* 93: 1639–1650.
18. Sot, J., M. Ibarguren, …, A. Alonso. 2008. Cholesterol displacement by ceramide in sphingomyelin-containing liquid-ordered domains, and generation of gel regions in giant lipidic vesicles. *FEBS Lett.* 582:3230–3236.
19. Chiantia, S., N. Kahya, …, P. Schwille. 2006. Effects of ceramide on liquid-ordered domains investigated by simultaneous AFM and FCS. *Biophys. J.* 90:4500–4508.
20. Ruiz-Argüello, M. B., G. Basáñez, …, A. Alonso. 1996. Different effects of enzyme-generated ceramides and diacylglycerols in phospholipid membrane fusion and leakage. *J. Biol. Chem.* 271:26616–26621.
21. Veiga, M. P., J. L. Arrondo, …, A. Alonso. 1999. Ceramides in phospholipid membranes: effects on bilayer stability and transition to nonlamellar phases. *Biophys. J.* 76:342–350.
22. Basáñez, G., M. B. Ruiz-Argüello, …, K. Edwards. 1997. Morphological changes induced by phospholipase C and by sphingomyelinase on large unilamellar vesicles: a cryo-transmission electron microscopy study of liposome fusion. *Biophys. J.* 72:2630–2637.
23. Montes, L. R., M. B. Ruiz-Argüello, …, A. Alonso. 2002. Membrane restructuring via ceramide results in enhanced solute efflux. *J. Biol. Chem.* 277:11788–11794.
24. Holopainen, J. M., M. I. Angelova, and P. K. Kinnunen. 2000. Vectorial budding of vesicles by asymmetrical enzymatic formation of ceramide in giant liposomes. *Biophys. J.* 78:830–838.
25. Ruiz-Argüello, M. B., M. P. Veiga, …, A. Alonso. 2002. Sphingomyelinase cleavage of sphingomyelin in pure and mixed lipid membranes. Influence of the physical state of the sphingolipid. *Chem. Phys. Lipids.* 114:11–20.
26. Kinnunen, P. K. 1991. On the principles of functional ordering in biological membranes. *Chem. Phys. Lipids.* 57:375–399.
27. Kinnunen, P. K., A. Kõiv, …, P. Mustonen. 1994. Lipid dynamics and peripheral interactions of proteins with membrane surfaces. *Chem. Phys. Lipids.* 73:181–207.
28. Fahy, E., S. Subramaniam, …, E. A. Dennis. 2005. A comprehensive classification system for lipids. *J. Lipid Res.* 46:839–861.
29. Pruett, S. T., A. Bushnev, …, A. H. Merrill, Jr. 2008. Biodiversity of sphingoid bases ("sphingosines") and related amino alcohols. *J. Lipid Res.* 49:1621–1639.
30. Merrill, A. H., Jr. 2002. De novo sphingolipid biosynthesis: a necessary, but dangerous, pathway. *J. Biol. Chem.* 277:25843–25846.
31. O'Brien, J. S., and G. Rouser. 1964. The fatty acid composition of brain sphingolipids: sphingomyelin, ceramide, cerebroside, and cerebroside sulfate. *J. Lipid Res.* 5:339–342.
32. Farwanah, H., B. Pierstorff, …, K. Sandhoff. 2007. Separation and mass spectrometric characterization of covalently bound skin ceramides using LC/APCI-MS and Nano-ESI-MS/MS. *J. Chromatogr. B Analyt. Technol. Biomed. Life Sci.* 852:562–570.
33. Hara, A., and T. Taketomi. 1975. Long chain base and fatty acid compositions of equine kidney sphingolipids. *J. Biochem.* 78:527–536.
34. Yasugi, E., T. Kasama, and Y. Seyama. 1991. Composition of long chain bases in ceramide of the guinea pig Harderian gland. *J. Biochem.* 110:202–206.
35. Ardail, D., I. Popa, …, J. Portoukalian. 2001. Occurrence of ceramides and neutral glycolipids with unusual long-chain base composition in purified rat liver mitochondria. *FEBS Lett.* 488:160–164.
36. Omae, F., M. Miyazaki, …, A. Suzuki. 2004. DES2 protein is responsible for phytoceramide biosynthesis in the mouse small intestine. *Biochem. J.* 379:687–695.
37. Mizutani, Y., A. Kihara, and Y. Igarashi. 2004. Identification of the human sphingolipid C4-hydroxylase, hDES2, and its up-regulation during keratinocyte differentiation. *FEBS Lett.* 563:93–97.
38. Chalfant, C. E., and S. Spiegel. 2005. Sphingosine 1-phosphate and ceramide 1-phosphate: expanding roles in cell signaling. *J. Cell Sci.* 118:4605–4612.
39. Gómez-Muñoz, A. 2006. Ceramide 1-phosphate/ceramide, a switch between life and death. *Biochim. Biophys. Acta.* 1758:2049–2056.
40. Renkonen, O., and E. L. Hirvisalo. 1969. Structure of plasma sphingadienine. *J. Lipid Res.* 10:687–693.
41. Panganamala, R. V., J. C. Geer, and D. G. Cornwell. 1969. Long-chain bases in the sphingolipids of atherosclerotic human aorta. *J. Lipid Res.* 10:445–455.
42. Pinto, S. N., L. C. Silva, …, M. Prieto. 2008. Membrane domain formation, interdigitation, and morphological alterations induced by the very long chain asymmetric C24:1 ceramide. *Biophys. J.* 95:2867–2879.
43. Megha, P., T. Sawatzki, …, E. London. 2007. Effect of ceramide *N*-acyl chain and polar headgroup structure on the properties of ordered lipid domains (lipid rafts). *Biochim. Biophys. Acta.* 1768:2205–2212.
44. Shah, J., J. M. Atienza, …, G. G. Shipley. 1995. Physical properties of ceramides: effect of fatty acid hydroxylation. *J. Lipid Res.* 36:1945–1955.
45. Jiménez-Rojo, N., A. B. García-Arribas, …, F. M. Goñi. 2014. Lipid bilayers containing sphingomyelins and ceramides of varying *N*-acyl lengths: a glimpse into sphingolipid complexity. *Biochim. Biophys. Acta.* 1838 (1 Pt B):456–464.
46. Dupuy, F. G., and B. Maggio. 2014. *N*-acyl chain in ceramide and sphingomyelin determines their mixing behavior, phase state, and surface topography in Langmuir films. *J. Phys. Chem. B.* 118:7475–7487.
47. Rerek, M. E., H. Chen, …, D. J. Moore. 2001. Phytosphingosine and sphingosine ceramide headgroup hydrogen bonding: structural insights through thermotropic hydrogen/deuterium exchange. *J. Phys. Chem. B.* 105:9355–9362.
48. Garidel, P. 2002. Calorimetric and spectroscopic investigations of phytosphingosine ceramide membrane organization. *Phys. Chem. Chem. Phys.* 4:1934–1942.
49. Kooijman, E. E., J. Sot, …, F. M. Goñi. 2008. Membrane organization and ionization behavior of the minor but crucial lipid ceramide-1-phosphate. *Biophys. J.* 94:4320–4330.
50. Morrow, M. R., A. Helle, …, J. M. Holopainen. 2009. Ceramide-1-phosphate, in contrast to ceramide, is not segregated into lateral lipid domains in phosphatidylcholine bilayers. *Biophys. J.* 96:2216–2226.
51. Silva, L. C., R. F. de Almeida, …, M. Prieto. 2007. Ceramide-domain formation and collapse in lipid rafts: membrane reorganization by an apoptotic lipid. *Biophys. J.* 92:502–516.
52. Sklar, L. A. 1980. The partition of *cis*-parinaric acid and *trans*-parinaric acid among aqueous, fluid lipid, and solid lipid phases. *Mol. Cell. Biochem.* 32:169–177.

53. Castro, B. M., L. C. Silva, …, M. Prieto. 2009. Cholesterol-rich fluid membranes solubilize ceramide domains: implications for the structure and dynamics of mammalian intracellular and plasma membranes. *J. Biol. Chem.* 284:22978–22987.

54. Megha, and E. London. 2004. Ceramide selectively displaces cholesterol from ordered lipid domains (rafts): implications for lipid raft structure and function. *J. Biol. Chem.* 279:9997–10004.

55. Alanko, S. M., K. K. Halling, …, B. Ramstedt. 2005. Displacement of sterols from sterol/sphingomyelin domains in fluid bilayer membranes by competing molecules. *Biochim. Biophys. Acta.* 1715:111–121.

56. Yu, C., M. Alterman, and R. T. Dobrowsky. 2005. Ceramide displaces cholesterol from lipid rafts and decreases the association of the cholesterol binding protein caveolin-1. *J. Lipid Res.* 46:1678–1691.

57. Staneva, G., C. Chachaty, …, P. J. Quinn. 2008. The role of sphingomyelin in regulating phase coexistence in complex lipid model membranes: competition between ceramide and cholesterol. *Biochim. Biophys. Acta.* 1778:2727–2739.

58. Busto, J. V., J. Sot, …, A. Alonso. 2010. Cholesterol displaces palmitoylceramide from its tight packing with palmitoylsphingomyelin in the absence of a liquid-disordered phase. *Biophys. J.* 99:1119–1128.

59. Pinto, S. N., F. Fernandes, …, M. Prieto. 2013. A combined fluorescence spectroscopy, confocal and 2-photon microscopy approach to re-evaluate the properties of sphingolipid domains. *Biochim. Biophys. Acta.* 1828:2099–2110.

60. Ali, M. R., K. H. Cheng, and J. Huang. 2006. Ceramide drives cholesterol out of the ordered lipid bilayer phase into the crystal phase in 1-palmitoyl-2-oleoyl-*sn*-glycero-3-phosphocholine/cholesterol/ceramide ternary mixtures. *Biochemistry.* 45:12629–12638.

61. Boulgaropoulos, B., M. Rappolt, …, G. Pabst. 2012. Lipid sorting by ceramide and the consequences for membrane proteins. *Biophys. J.* 102:2031–2038.

62. Nyholm, T. K., P. M. Grandell, …, J. P. Slotte. 2010. Sterol affinity for bilayer membranes is affected by their ceramide content and the ceramide chain length. *Biochim. Biophys. Acta.* 1798:1008–1013.

63. Björkqvist, Y. J., T. K. Nyholm, …, B. Ramstedt. 2005. Domain formation and stability in complex lipid bilayers as reported by cholestatrienol. *Biophys. J.* 88:4054–4063.

64. Maula, T., B. Westerlund, and J. P. Slotte. 2009. Differential ability of cholesterol-enriched and gel phase domains to resist benzyl alcohol-induced fluidization in multilamellar lipid vesicles. *Biochim. Biophys. Acta.* 1788:2454–2461.

65. Cohen, R., Y. Barenholz, …, A. Dagan. 1984. Preparation and characterization of well defined D-erythro sphingomyelins. *Chem. Phys. Lipids.* 35:371–384.

66. Kuklev, D. V., and W. L. Smith. 2004. Synthesis of four isomers of parinaric acid. *Chem. Phys. Lipids.* 131:215–222.

67. Fischer, R. T., F. A. Stephenson, …, F. Schroeder. 1984. delta 5,7,9(11)-Cholestatrien-3 beta-ol: a fluorescent cholesterol analogue. *Chem. Phys. Lipids.* 36:1–14.

68. Lakowicz, J. R. 1999. Principles of Fluorescence Spectroscopy. Kluwer Academic/Plenum Publishers, New York.

69. Busto, J. V., M. L. Fanani, …, A. Alonso. 2009. Coexistence of immiscible mixtures of palmitoylsphingomyelin and palmitoylceramide in monolayers and bilayers. *Biophys. J.* 97:2717–2726.

70. Maula, T., M. Kurita, …, J. P. Slotte. 2011. Effects of sphingosine 2*N*- and 3*O*-methylation on palmitoyl ceramide properties in bilayer membranes. *Biophys. J.* 101:2948–2956.

71. Maula, T., I. Artetxe, …, J. P. Slotte. 2012. Importance of the sphingoid base length for the membrane properties of ceramides. *Biophys. J.* 103:1870–1879.

72. Artetxe, I., C. Sergelius, …, T. Maula. 2013. Effects of sphingomyelin headgroup size on interactions with ceramide. *Biophys. J.* 104:604–612.

73. Jaikishan, S., and J. P. Slotte. 2013. Stabilization of sphingomyelin interactions by interfacial hydroxyls - a study of phytosphingomyelin properties. *Biochim. Biophys. Acta.* 1828:391–397.

74. Löfgren, H., and I. Pascher. 1977. Molecular arrangements of sphingolipids. The monolayer behaviour of ceramides. *Chem. Phys. Lipids.* 20:273–284.

75. Ekholm, O., S. Jaikishan, …, J. P. Slotte. 2011. Membrane bilayer properties of sphingomyelins with amide-linked 2- or 3-hydroxylated fatty acids. *Biochim. Biophys. Acta.* 1808:727–732.

76. Pascher, I. 1976. Molecular arrangements in sphingolipids. Conformation and hydrogen bonding of ceramide and their implication on membrane stability and permeability. *Biochim. Biophys. Acta.* 455:433–451.

77. Shah, J., J. M. Atienza, …, G. G. Shipley. 1995. Structural and thermotropic properties of synthetic C16:0 (palmitoyl) ceramide: effect of hydration. *J. Lipid Res.* 36:1936–1944.

78. Sot, J., F. J. Aranda, …, A. Alonso. 2005. Different effects of long- and short-chain ceramides on the gel-fluid and lamellar-hexagonal transitions of phospholipids: a calorimetric, NMR, and x-ray diffraction study. *Biophys. J.* 88:3368–3380.

79. Marsh, D. 1999. Thermodynamic analysis of chain-melting transition temperatures for monounsaturated phospholipid membranes: dependence on cis-monoenoic double bond position. *Biophys. J.* 77:953–963.

80. Brockman, H. L., M. M. Momsen, …, R. Bittman. 2004. The 4,5-double bond of ceramide regulates its dipole potential, elastic properties, and packing behavior. *Biophys. J.* 87:1722–1731.

81. Li, L., X. Tang, …, M. C. Yappert. 2002. Conformational characterization of ceramides by nuclear magnetic resonance spectroscopy. *Biophys. J.* 82:2067–2080.

82. Nyholm, T. K., D. Lindroos, …, J. P. Slotte. 2011. Construction of a DOPC/PSM/cholesterol phase diagram based on the fluorescence properties of *trans*-parinaric acid. *Langmuir.* 27:8339–8350.

83. Sklar, L. A., G. P. Miljanich, and E. A. Dratz. 1979. Phospholipid lateral phase separation and the partition of *cis*-parinaric acid and *trans*-parinaric acid among aqueous, solid lipid, and fluid lipid phases. *Biochemistry.* 18:1707–1716.

84. Maula, T., B. Urzelai, and J. Peter Slotte. 2011. The effects of *N*-acyl chain methylations on ceramide molecular properties in bilayer membranes. *Eur. Biophys. J.* 40:857–863.

85. Marsh, D. 2009. Cholesterol-induced fluid membrane domains: a compendium of lipid-raft ternary phase diagrams. *Biochim. Biophys. Acta.* 1788:2114–2123.

86. de Almeida, R. F., A. Fedorov, and M. Prieto. 2003. Sphingomyelin/phosphatidylcholine/cholesterol phase diagram: boundaries and composition of lipid rafts. *Biophys. J.* 85:2406–2416.

87. Busto, J. V., A. B. García-Arribas, …, A. Alonso. 2014. Lamellar gel ($l\beta$) phases of ternary lipid composition containing ceramide and cholesterol. *Biophys. J.* 106:621–630.

88. Wang, T. Y., and J. R. Silvius. 2003. Sphingolipid partitioning into ordered domains in cholesterol-free and cholesterol-containing lipid bilayers. *Biophys. J.* 84:367–378.

89. Koynova, R., and M. Caffrey. 1998. Phases and phase transitions of the phosphatidylcholines. *Biochim. Biophys. Acta.* 1376:91–145.

Supplemental information

Influence of Hydroxylation, Chain Length, and Chain Unsaturation on Bilayer Properties of Ceramides

Terhi Maula*, Md. Abdullah Al Sazzad, J. Peter Slotte

Biochemistry, Faculty of Science and Engineering, Åbo Akademi University, 20520 Turku, Finland

*Corresponding author

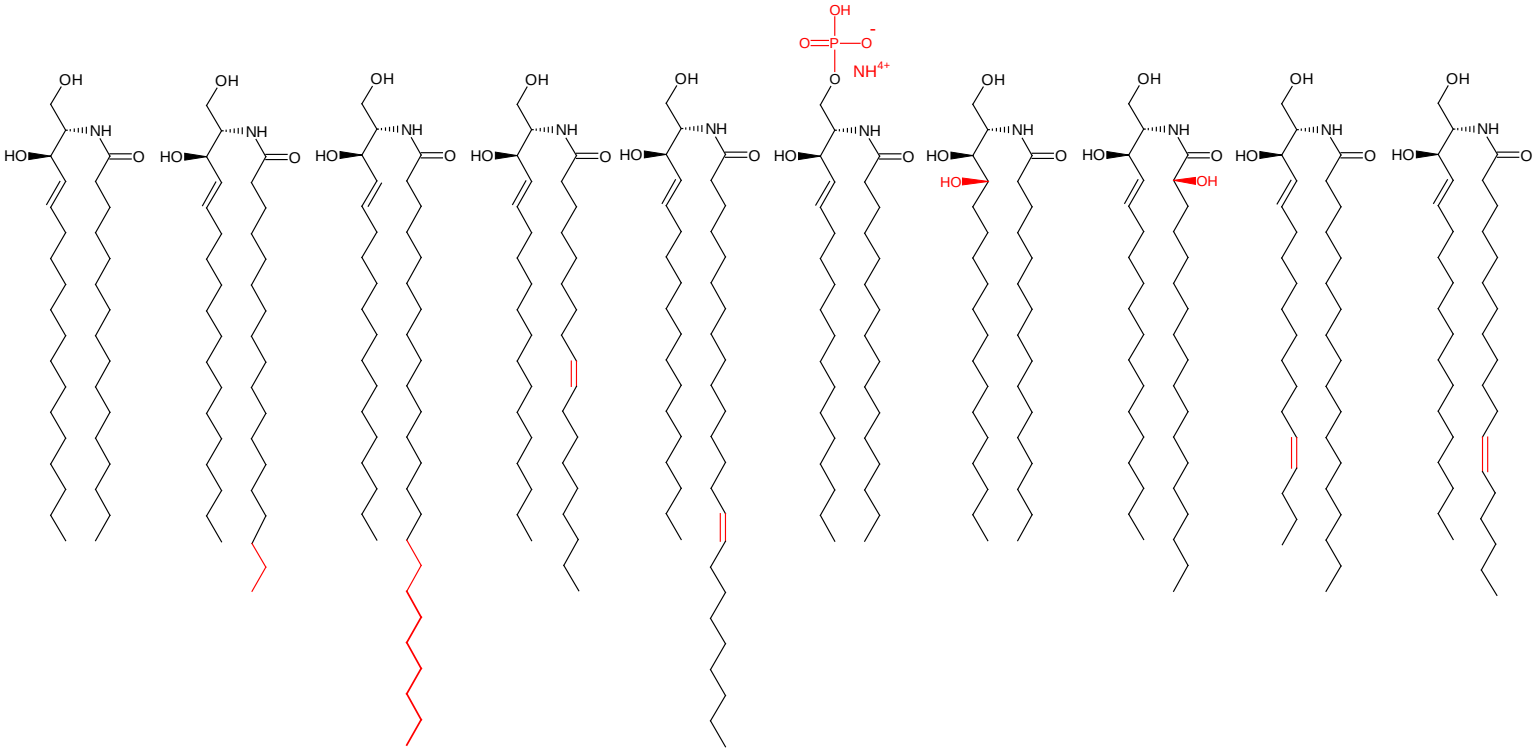

Scheme S1. Molecular structures of (from left to right) C16-cer, C18-cer, C24-cer, C18:1$^{\Delta 9c}$-cer, C24:1$^{\Delta 15c}$-cer, Cer-1-P, C16-phyto-cer, C18^{2OH}-cer, C18-sphingadiene-cer and C18:1$^{\Delta 12c}$-cer.

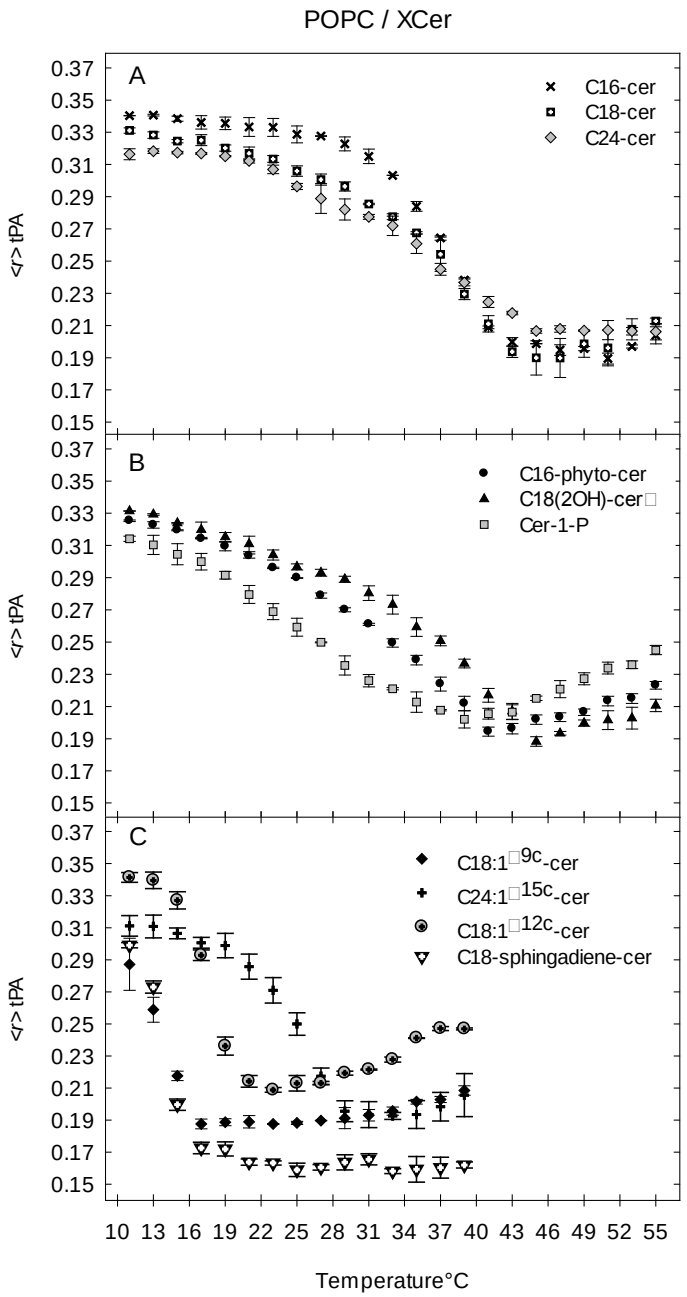

Figure S1. Steady-state fluorescence anisotropy of tPA (1 mol%) as a function of temperature in POPC/XCer bilayers (60:15 by mol). N=2-3 ± SD.

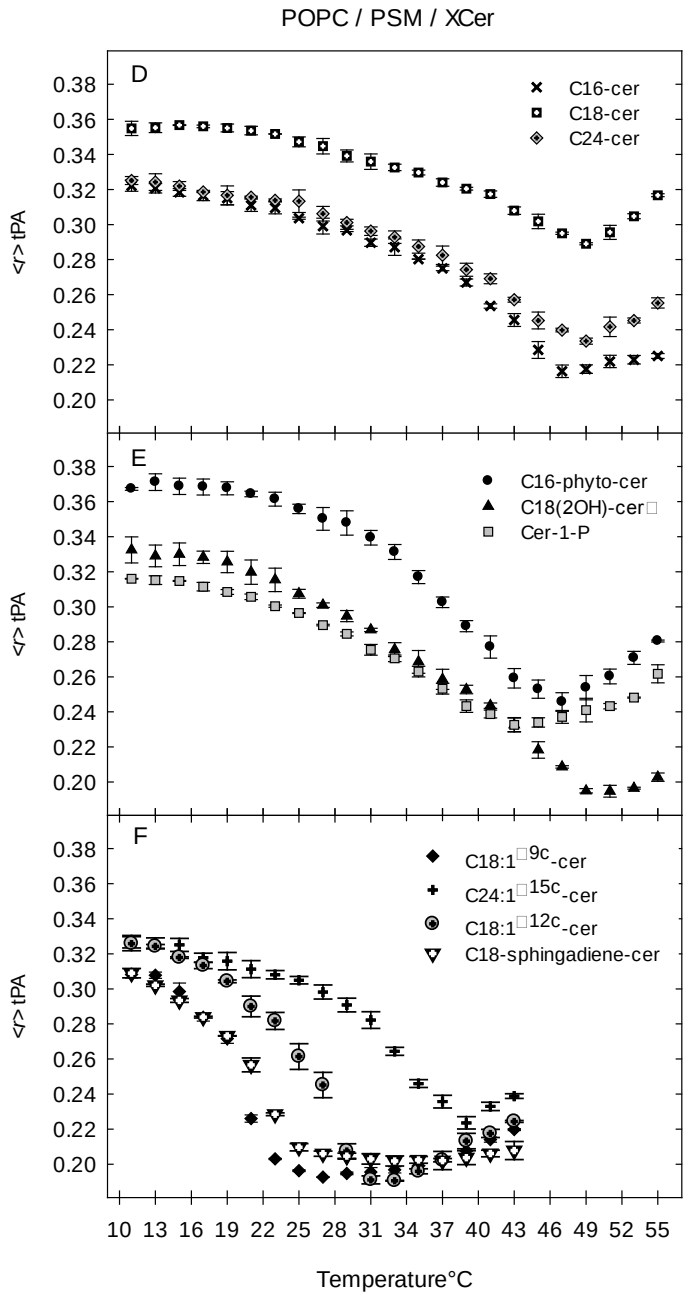

Figure S2. Steady-state fluorescence anisotropy of tPA (1 mol%) as a function of temperature in POPC/PSM/XCer bilayers (60:15:15 by mol). N=2-3 ± SD.

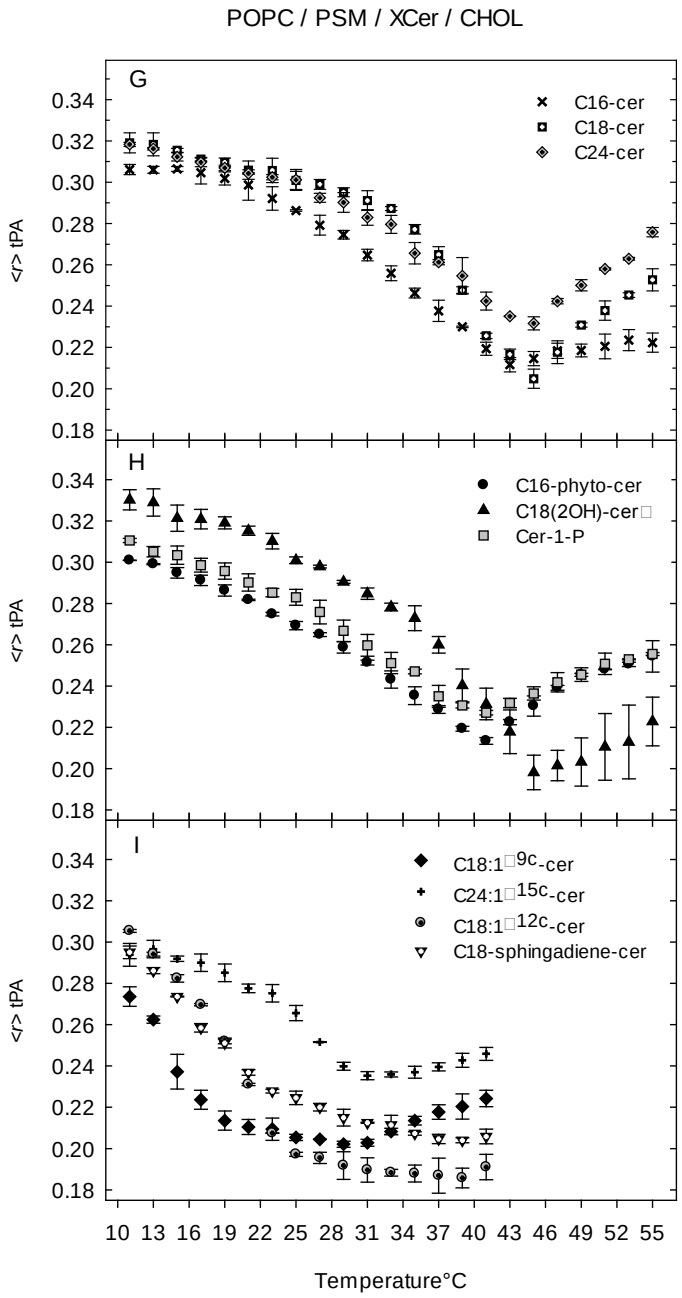

Figure S3. Steady-state fluorescence anisotropy of tPA (1 mol%) as a function of temperature in POPC/PSM/XCer/Chol bilayers (60:15:15:10 by mol). N=2-3 ± SD.

Table S1. Time-resolved fluorescence decays of tPA (1 mol%) in binary and ternary mixed bilayers at 23°C.

Sample	τ_1	f_1	α_1	τ_2	f_2	α_2	τ_3	f_3	α_3	τ_{AV}
POPC/C16-cer	49.1 ± 2.6	38.7 ± 3.1	14.8 ± 1.1	27.4 ± 0.7	45.0 ± 3.1	30.8 ± 2.1	5.6 ± 0.1	16.2 ± 1.4	54.2 ± 1.7	32.3 ± 1.9
POPC/C18-cer	49.0 ± 2.2	38.6 ± 3.0	14.6 ± 1.4	28.0 ± 1.1	45.0 ± 3.2	29.8 ± 2.1	5.4 ± 0.1	16.3 ± 0.8	55.4 ± 1.5	32.4 ± 2.4
POPC/C24-cer	48.2 ± 0.1	38.6 ± 1.3	15.7 ± 0.8	27.4 ± 0.1	46.8 ± 1.2	33.4 ± 0.3	5.6 ± 0.1	14.6 ± 0.1	50.9 ± 0.4	32.2 ± 0.3
POPC/C16-phyto-cer	42.0 ± 1.7	33.0 ± 1.5	7.5 ± 0.9	19.1 ± 1.7	18.2 ± 1.0	9.1 ± 0.4	5.5 ± 0.04	48.7 ± 2.5	83.3 ± 1.2	20.0 ± 0.4
POPC/C18(2OH)-cer	52.1 ± 3.7	43.5 ± 6.7	15.7 ± 2.3	29.7 ± 1.0	39.0 ± 6.3	24.6 ± 3.1	5.4 ± 0.04	17.3 ± 0.4	59.6 ± 1.7	35.4 ± 2.9
POPC/Cer-1- P	44.1 ± 2.5	39.3 ± 2.7	9.6 ± 1.5	19.6 ± 2.7	20.0 ± 2.4	11.0 ± 0.7	5.5 ± 0.05	40.6 ± 3.9	79.2 ± 2.3	23.5 ± 1.7
POPC/C18:1$^{\Delta 9c}$-cer	8.5 ± 0.2	32.7 ± 2.3	23.5 ± 2.0	5.3 ± 0.1	67.2 ± 2.3	76.5 ± 2.0				6.3 ± 0.09
POPC/C24:1$^{\Delta 15c}$-cer	37.8 ± 1.2	26.7 ± 3.2	8.1 ± 1.2	20.7 ± 1.0	40.0 ± 5.0	23.1 ± 3.4				20.1 ± 1.6
POPC/C18:1$^{\Delta 12c}$-cer	10.7 ± 0.5	14.8 ± 2.6	8.7 ± 1.3	5.9 ± 0.1	85.2 ± 2.6	91.2 ± 1.4				6.6 ± 0.1
POPC/C18-sphingadiene-cer	9.3 ± 0.4	25.1 ± 0.6	16.7 ± 0.8	5.5 ± 0.1	74.8 ± 0.6	83.2 ± 0.8				6.5 ± 0.1
POPC/PSM/C16-cer	52.5 ± 3.7	49.2 ± 2.6	16.7 ± 1.4	26.5 ± 1.5	31.1 ± 2.5	21.0 ± 2.6	5.6 ± 0.1	19.6 ± 2.9	62.2 ± 3.8	35.2 ± 3.4
POPC/PSM/C18-cer	49.3 ± 5.0	44.6 ± 3.8	18.0 ± 1.8	25.5 ± 1.9	40.9 ± 2.8	32.0 ± 2.3	5.6 ± 0.2	14.3 ± 1.7	49.9 ± 2.8	33.4 ± 4.3
POPC/PSM/C24-cer	48.0 ± 5.6	38.8 ± 8.9	17.4 ± 5.0	24.7 ± 1.7	49.0 ± 6.9	42.2 ± 5.6	6.2 ± 0.1	12.1 ± 3.5	40.3 ± 7.0	31.8 ± 5.8
POPC/PSM/C16-phyto-cer	47.9 ± 1.1	41.0 ± 0.6	9.6 ± 0.7	20.8 ± 2.0	20.0 ± 3.2	10.8 ± 1.6	5.4 ± 0.1	38.9 ± 3.7	79.5 ± 2.4	26.0 ± 1.7
POPC/PSM/ C18(2OH)-cer	52.4 ± 6.5	47.9 ± 2.7	18.9 ± 1.7	27.6 ± 2.9	37.4 ± 1.9	28.1 ± 2.7	5.7 ± 0.2	14.6 ± 2.3	52.8 ± 4.1	36.3 ± 5.3
POPC/PSM/Cer-1-P	49.0 ± 2.5	43.5 ± 1.7	12.2 ± 1.4	22.8 ± 2.3	26.0 ± 3.0	15.6 ± 2.2	5.7 ± 0.1	30.3 ± 4.5	72.2 ± 3.6	29.1 ± 3.0
POPC/PSM/C18:1$^{\Delta 9c}$-cer	34.9 ± 0.1	21.3 ± 0.5	5.5 ± 0.1	15.9 ± 0.4	25.6 ± 0.5	14.7 ± 0.1	6.0 ± 0.1	52.9 ± 1.0	79.7 ± 0.07	14.8 ± 0.2
POPC/PSM/C24:1$^{\Delta 15c}$-cer	39.3 ± 2.3	30.5 ± 5.6	10.7 ± 1.6	19.7 ± 2.4	47.7 ± 4.2	33.5 ± 1.8	5.4 ± 0.9	21.7 ± 1.7	55.7 ± 0.2	22.5 ± 0.8
POPC/PSM/C18:1$^{\Delta 12c}$-cer	38.1 ± 2.8	28.4 ± 8.1	8.6 ± 3.2	18.5 ± 2.4	38.0 ± 1.8	23.7 ± 4.9	5.5 ± 0.7	33.4 ± 9.6	67.6 ± 8.1	19.6 ± 1.0
POPC/PSM/C18-sphingadiene-cer	37.1 ± 1.8	24.8 ± 7.1	6.7 ± 2.4	16.6 ± 2.3	31.0 ± 3.7	18.9 ± 5.7	5.7 ± 0.7	44.0 ± 10.8	74.3 ± 8.1	16.9 ± 1.1

The bilayer composition was 60/15 (by mol) and 60/15/15 (by mol) for the binary and ternary mixtures, respectively. Each value is the average of at least three independently repeated experiments (±SD). τ, lifetime (ns); f, fractional intensity (%); α, fractional amplitude (%); τ_{AV}, intensity-weighted average lifetime (ns).

Table S2. Time-resolved fluorescence decays of tPA (1 mol%) in binary and ternary mixed bilayers at 10°C.

Sample	τ_1	f_1	α_1	τ_2	f_2	α_2	τ_3	f_3	α_3	τ_{AV}
POPC/C18:1$^{\Delta 9c}$-cer	50.3 ± 2.0	42.7 ± 3.5	21.5 ± 1.2	27.9 ± 1.8	44.0 ± 5.8	40.0 ± 5.8	8.7 ± 0.4	13.2 ± 2.5	38.4 ± 5.0	35.0 ± 1.7
POPC/C24:1$^{\Delta 15c}$-cer	51.7 ± 1.4	48.4 ± 5.7	25.5 ± 4.0	28.9 ± 1.6	40.0 ± 4.6	37.5 ± 2.1	8.4 ± 0.5	11.5 ± 1.2	36.9 ± 2.6	37.6 ± 1.9
POPC/C18:1$^{\Delta 12c}$-cer	53.1 ± 2.0	45.6 ± 4.2	24.8 ± 1.3	29.8 ± 2.1	44.9 ± 5.6	43.6 ± 5.6	8.7 ± 0.5	9.5 ± 1.4	31.4 ± 4.3	38.4 ± 1.2
POPC/C18-sphingadiene-cer	50.6 ± 1.7	47.6 ± 1.3	21.9 ± 1.9	25.0 ± 2.6	35.7 ± 3.4	33.4 ± 3.6	8.5 ± 0.4	16.5 ± 2.9	44.6 ± 5.1	34.5 ± 2.3
POPC/PSM/C18:1$^{\Delta 9c}$-cer	52.4 ± 1.2	43.0 ± 3.1	23.2 ± 1.5	29.0 ± 0.6	47.2 ± 3.3	46.0 ± 2.6	8.8 ± 0.3	9.6 ± 0.2	30.7 ± 1.2	37.2 ± 1.2
POPC/PSM/C24:1$^{\Delta 15c}$-cer	53.1 ± 0.8	45.2 ± 3.0	23.5 ± 1.9	28.4 ± 0.8	44.1 ± 2.5	42.6 ± 1.3	8.6 ± 0.2	10.6 ± 0.4	33.8 ± 0.8	37.4 ± 0.1
POPC/PSM/C18:1$^{\Delta 12c}$-cer	51.6 ± 2.4	50.0 ± 4.9	26.7 ± 1.1	27.2 ± 2.6	42.4 ± 4.2	43.1 ± 4.3	7.1 ± 2.8	7.5 ± 1.4	30.0 ± 3.1	37.9 ± 1.2
POPC/PSM/C18-sphingadiene-cer	52.4 ± 3.6	48.3 ± 7.7	25.8 ± 3.7	27.3 ± 4.0	43.9 ± 7.0	45.4 ± 8.3	7.8 ± 2.5	7.7 ± 3.1	28.6 ± 9.2	37.9 ± 2.2

The bilayer composition was 60/15 (by mol) and 60/15/15 (by mol) for the binary and ternary mixtures, respectively. Each value is the average of at least three independently repeated experiments (±SD). τ, lifetime (ns); f, fractional intensity (%); α, fractional amplitude (%); τ_{AV}, intensity-weighted average lifetime (ns).

Table S3. Time-resolved fluorescence decays of tPA (1 mol%, 23 ^{o}C) in complex mixed bilayers containing cholesterol.

Sample	τ_1	f_1	α_1	τ_2	f_2	α_2	τ_3	f_3	α_3	τ_{AV}
POPC/PSM/C16-cer/CHOL	50.3 ± 1.0	36.3 ± 9.5	10.7 ± 1.9	21.9 ± 3.7	31.1 ± 7.3	21.5 ± 4.4	7.3 ± 1.3	32.5 ± 2.4	67.6 ± 2.4	27.7 ± 2.4
POPC/PSM/C18-cer/CHOL	47.5 ± 2.8	35.8 ± 2.1	12.30 ± 0.7	22.3 ± 1.2	37.1 ± 2.8	27.29 ± 4.6	7.3 ± 0.7	27.0 ± 0.9	60.4 ± 5.2	27.3 ± 1.5
POPC/PSM/C24-cer/CHOL	44.1 ± 3.6	35.1 ± 4.26	13.3 ± 2.2	21.1 ± 2.8	42.5 ± 1.6	33.6 ± 2.3	7.0 ± 0.8	22.3 ± 3.3	53.0 ± 4.5	26.0 ± 1.4
POPC/PSM/C16-phyto-cer/CHOL	43.8 ± 0.3	18.0 ± 6.3	4.2 ± 1.4	15.5 ± 0.7	36.5 ± 8.8	24.4 ± 6.6	6.5 ± 0.2	45.3 ± 2.5	71.3 ± 5.1	16.5 ± 1.8
POPC/PSM/C18(2OH)-cer/CHOL	47.6 ± 2.5	40.6 ± 1.1	14.6 ± 1.6	22.4 ± 1.3	33.8 ± 4.9	26.0 ± 5.0	7.3 ± 0.4	25.5 ± 3.9	59.3 ± 6.6	28.8 ± 0.7
POPC/PSM/Cer-1- P/CHOL	50.0 ± 0.4	26.8 ± 4.8	6.9 ± 1.2	17.2 ± 0.3	35.8 ± 5.1	27.0 ± 3.9	7.4 ± 0.4	37.4 ± 0.6	65.9 ± 2.6	22.3 ± 1.2
POPC/PSM/C18:1$^{\Delta 9c}$-cer/CHOL	12.7 ± 0.4	52.7 ± 2.0	37.6 ± 1.9	6.9 ± 0.2	47.3 ± 2.0	62.3 ± 1.9				9.9 ± 0.4
POPC/PSM/C24:1$^{\Delta 15c}$-cer/CHOL	39.1 ± 3.1	16.4 ± 4.2	5.4 ± 1.9	18.7 ± 0.8	47.4 ± 4.5	32.2 ± 0.6	7.4 ± 0.5	36.1 ± 0.3	62.2 ± 1.4	17.9 ± 0.1
POPC/PSM/C18:1$^{\Delta 12c}$-cer/CHOL	13.8 ± 0.8	43.7 ± 3.2	28.0 ± 2.9	6.9 ± 0.3	56.3 ± 3.3	72.0 ± 2.9				9.9 ± 0.5
POPC/PSM/C18-sphingadiene-cer/CHOL	12.9 ± 0.6	48.4 ± 3.7	32.5 ± 3.6	6.6 ± 0.5	51.6 ± 3.7	67.5 ± 3.6				9.7 ± 0.7

The bilayer composition was 60/15/15/10 (by mol) for the quaternary mixtures. Each value is the average of at least three independently repeated experiments (±SD). τ, lifetime (ns); f, fractional intensity (%); α, fractional amplitude (%); τ_{AV}, intensity-weighted average lifetime (ns).

Table S4. Time-resolved fluorescence decays of tPA (1 mol%, 10 ^{o}C) in complex mixed bilayers containing cholesterol.

Sample	τ_1	f_1	α_1	τ_2	f_2	α_2	τ_3	f_3	α_3	τ_{AV}
POPC/PSM/C18:1$^{\Delta 9c}$-cer/CHOL	48.5 ± 2.2	28.0 ± 0.5	13.7 ± 0.9	24.4 ± 1.7	60.1 ± 2.5	58.3 ± 4.3	6.5 ± 4.8	11.7 ± 2.4	27.9 ± 4.6	29.5 ± 1.5
POPC/PSM/C24:1$^{\Delta 15c}$-cer/CHOL	45.7 ± 3.5	45.0 ± 7.2	22.2 ± 3.0	21.5 ± 3.3	46.5 ± 5.0	48.7 ± 2.7	6.6 ± 2.3	8.5 ± 2.2	29.0 ± 0.3	31.1 ± 1.2
POPC/PSM/C18:1$^{\Delta 12c}$-cer/CHOL	50.7 ± 0.9	31.8 ± 7.8	14.9 ± 5.8	23.7 ± 3.3	55.2 ± 3.6	53.2 ± 2.8	9.0 ± 0.9	12.9 ± 4.7	31.9 ± 7.2	30.4 ± 4.9
POPC/PSM/C18-sphingadiene-cer/CHOL	47.6 ± 3.3	29.2 ± 3.8	12.9 ± 3.4	22.1 ± 1.5	57.9 ± 2.2	54.2 ± 4.2	7.9 ± 0.5	12.9 ± 4.5	32.7 ± 47.2	27.7 ± 2.0

The bilayer composition was 60/15/15/10 (by mol) for the quaternary mixtures. Each value is the average of at least three independently repeated experiments (±SD). τ, lifetime (ns); f, fractional intensity (%); α, fractional amplitude (%); τ_{AV}, intensity-weighted average lifetime (ns).